

A TIME-DEPENDENT MANY-ELECTRON APPROACH
TO ATOMIC AND MOLECULAR INTERACTIONS

By

KEITH RUNGE

A DISSERTATION PRESENTED TO THE GRADUATE SCHOOL
OF THE UNIVERSITY OF FLORIDA IN PARTIAL FULFILLMENT
OF THE REQUIREMENTS FOR THE DEGREE OF
DOCTOR OF PHILOSOPHY

UNIVERSITY OF FLORIDA

1993

To James A. Lines and his desk

ACKNOWLEDGEMENTS

I would like to thank my colleagues at the Quantum Theory Project of the University of Florida. I would particularly like to thank my thesis advisor Dr. David A. Micha and the other members of his group with whom I have been involved, Dr. Deepak Srivastava, Dr. Zaida Parra, Dr. Cliff Stodden, Dr. Eric Q. Feng, Dr. Joel Cohen, Robert Asher, Dario Beksic, Dr. Herbert Da Costa, Dr. Salvador Miret-Artes, Dr. Dario Rojas, and Jorge Morales. I have had many helpful conversations with many of the members of the members of QTP and the Physics Department. I thank them all and in particular Dr. Jim Fry, Dr. John Stanton, Dr. Hugh "da man" Taylor, Dr. Walt Lauderdale, David Bernholdt, and Ajith Perera. Special mention for many extended and insightful conversations is due Dr. Agustín Díz.

My deep appreciation is expressed to the members of University Lutheran Church, who among other things, helped me weather the tornado of March 22, 1986. I particularly mention Rev. Robert Carr and Rev. Jack Saarela as good friends and as representatives of the congregation. Thanks are due to all those who are willing to engage in athletic contests, particularly, Dr. Mark Meisel,

Roger Merkel, "Frybaby," Erika Kisvarsanyi, Dr. Peter Andersen, Vince Lane,
and Mark Montoya.

Finally, I wish to thank my family for all their support.

TABLE OF CONTENTS

ACKNOWLEDGEMENTS	iii
LIST OF TABLES	vii
LIST OF FIGURES	viii
ABSTRACT.....	xii
CHAPTERS	
1. INTRODUCTION	1
Overview of Theoretical Methods	1
Outline of the Thesis	8
2. COUPLING OF ELECTRONIC AND NUCLEAR MOTIONS	11
3. THE TIME-DEPENDENT HARTREE-FOCK EQUATIONS	16
4. TEMPORAL LINEARIZATION OF THE TIME-DEPENDENT HARTREE-FOCK EQUATIONS	21
5. TIME-DEPENDENT ELECTRONIC ALIGNMENT AND POPULATION ANALYSES	27
6. INTEGRATION OF THE LINEARIZED TDHF EQUATIONS ..	34
7. CHOICE OF BASIS SET AND ITS EFFECT ON CALCULATION ..	38
8. APPLICATIONS I: THE PROTON-HYDROGEN ATOM SYSTEM	50
Overview of Experimental Methods	50
Integral Cross Sections	52
Differential Cross Sections	63
Time-dependent Properties	69
9. APPLICATIONS II: THE HELIUM(2+)-HYDROGEN ATOM SYSTEM	84
10. APPLICATIONS III: THE HYDROGEN ATOM-HYDROGEN ATOM SYSTEM	94

11. CONCLUSIONS AND DISCUSSION	107
A. CALCULATION OF OVERLAP AND HAMILTONIAN MATRIX ELEMENTS IN THE HYDROGENIC BASIS	112
B. CALCULATION OF ONE-ELECTRON INTEGRALS OVER GAUSSIANS INCLUDING ELECTRON TRANSLATION FACTORS	120
C. FLOW CHART OF THE TIME-DEPENDENT DENSITY MATRIX COMPUTER PROGRAM	128
REFERENCES	129
BIOGRAPHICAL SKETCH	134

LIST OF TABLES

<u>Table</u>	<u>page</u>
8.1: A comparison of experiment and theory for total integral cross sections.....	54
8.2: Comparison of theoretical and experimental results for state-to-state integral cross sections for a 2 keV proton incident on a Hydrogen atom.	60
8.3: Comparison of theoretical and experimental results for integral alignments in proton-Hydrogen atom collisions	61
9.1: A comparison of experiment and theory of charge transfer integral cross section	86
9.2: Comparison of theoretical and experimental results for state-to-state integral cross section for an 8 keV He^{2+} projectile incident on a Hydrogen atom.	87
10.1: A comparison of experiment and theory for excitation integral cross section at 1 keV.....	97

LIST OF FIGURES

<u>Figure</u>	<u>page</u>
5-1: The collision is taken to occur in the x-z plane.	28
7-1: Transfer probability vs. Impact parameter in au for proton-Hydrogen atom collisions at a lab energy of 1 keV. (full line: including ETFs, dotted line: without ETFs)	40
7-2: Transfer probability vs. Impact parameter in au for proton-Hydrogen atom collisions at a lab energy of 10 eV. (full line: including ETFs, dotted line: without ETFs)	41
7-3: Electron transfer probability vs. Impact parameter in au (plus: exact 1s hydrogenic; triangle: 3 Gaussians; diamond: 4 Gaussians; box: 5 Gaussians; cross: 6 Gaussians)	46
8-1: Transfer probability vs Impact parameter in au for a 1 keV proton-Hydrogen atom collision (plus: zero potential; circle: Coulomb potential; cross: screened Coulomb potential)	55
8-2: Transfer probability vs Impact parameter in au for a 100 eV proton-Hydrogen atom collision (plus: zero potential; circle: Coulomb potential; cross: screened Coulomb potential)	56
8-3: Transfer probability vs Impact parameter in au for a 10 eV proton-Hydrogen atom collision (plus: zero potential; circle: Coulomb potential; cross: screened Coulomb potential)	57
8-4: Total integral cross section vs Projectile energy (eV) comparison between our theoretical results and those of experiment	59
8-5: Elastic reduced differential cross section vs lab angle for a 410 eV proton incident on a Hydrogen atom target {full line: SCP; dotted line: CP; triangles: [65] }	64

<u>Figure</u>	<u>page</u>
8-6: Charge transfer reduced differential cross section vs lab angle for a 410 eV proton incident on a Hydrogen atom target {full line: SCP; dotted line: CP; triangles: [65] }	65
8-7: Elastic and charge transfer reduced differential cross section vs lab angle for a 500 eV proton incident on a Hydrogen atom target {full line: elastic; dotted line: charge transfer; triangles: experimental elastic; diamonds: experimental charge transfer; experimental results from [65]}	67
8-8: Elastic and charge transfer reduced differential cross section vs lab angle for a 700 eV proton incident on a Hydrogen atom target {full line: elastic; dotted line: charge transfer; triangles: experimental elastic; diamonds: experimental charge transfer; experimental results from [65]}	68
8-9: Mulliken population of the target 1s state vs time in au in a 1 keV proton-Hydrogen atom collision, at $b=0.2$ au	70
8-10: Löwdin population of the target 1s state vs time in au in a 1 keV proton-Hydrogen atom collision, at $b=0.2$ au	71
8-11: Löwdin population of the target 2s state vs time in au in a 1 keV proton-Hydrogen atom collision, at $b=0.2$ au	72
8-12: Löwdin population of the target $2p_x$ state vs time in au in a 1 keV proton-Hydrogen atom collision, at $b=0.2$ au	73
8-13: Löwdin population of the target $2p_z$ state vs time in au in a 1 keV proton-Hydrogen atom collision, at $b=0.2$ au	74
8-14: Löwdin population of the projectile 1s state vs time in au in a 1 keV proton-Hydrogen atom collision, at $b=0.2$ au	75
8-15: Löwdin population of the projectile 2s state vs time in au in a 1 keV proton-Hydrogen atom collision, at $b=0.2$ au	76

<u>Figure</u>	<u>page</u>
8-16: Löwdin population of the projectile $2p_x$ state vs time in au in a 1 keV proton-Hydrogen atom collision, at $b=0.2$ au	77
8-17: Löwdin population of the projectile $2p_z$ state vs time in au in a 1 keV proton-Hydrogen atom collision, at $b=0.2$ au	78
8-18: Löwdin population of the target 1s state vs time in au in a 10 eV proton-Hydrogen atom collision, at $b=1.0$ au	80
8-19: Löwdin population of the target 1s state vs time in au in a 10 eV proton-Hydrogen atom collision, at $b=1.2$ au	81
8-20: Alignment parameter vs time in au in a 1 keV proton-Hydrogen atom collision, at $b=0.2$ au	83
9-1: Löwdin population of the target 1s state vs time in au in a 4 keV He^{2+} -Hydrogen atom collision at $b=0.2$ au	89
9-2: Löwdin population of the projectile 2s state vs time in au in a 4 keV He^{2+} -Hydrogen atom collision at $b=0.2$ au	90
9-3: Löwdin population of the projectile $2p_x$ state vs time in au in a 4 keV He^{2+} -Hydrogen atom collision at $b=0.2$ au	91
9-4: Löwdin population of the projectile $2p_z$ state vs time in au in a 4 keV He^{2+} -Hydrogen atom collision at $b=0.2$ au	92
9-5: Alignment parameter vs time in au in a 4 keV He^{2+} -Hydrogen atom collision at $b=0.2$ au	93
10-1: Löwdin population for alpha spin of the target 1s state vs time in au for a 1 keV Hydrogen atom-Hydrogen atom collision, at $b=0.2$ au . .	99
10-2: Löwdin population for alpha spin of the target 2s state vs time in au for a 1 keV Hydrogen atom-Hydrogen atom collision, at $b=0.2$ au .	100

<u>Figure</u>	<u>page</u>
10-3: Löwdin population for alpha spin of the target $2p_x$ state vs time in au for a 1 keV Hydrogen atom-Hydrogen atom collision, at $b=0.2$ au .	101
10-4: Löwdin population for alpha spin of the target $2p_z$ state vs time in au for a 1 keV Hydrogen atom-Hydrogen atom collision, at $b=0.2$ au .	102
10-5: Löwdin population for alpha spin of the projectile $1s$ state vs time in au for a 1 keV Hydrogen atom-Hydrogen atom collision, at $b=0.2$ au .	103
10-6: Löwdin population for alpha spin of the projectile $2s$ state vs time in au for a 1 keV Hydrogen atom-Hydrogen atom collision, at $b=0.2$ au .	104
10-7: Löwdin population for alpha spin of the projectile $2p_x$ state vs time in au for a 1 keV Hydrogen atom-Hydrogen atom collision, at $b=0.2$ au .	105
10-8: Löwdin population for alpha spin of the projectile $2p_z$ state vs time in au for a 1 keV Hydrogen atom-Hydrogen atom collision, at $b=0.2$ au .	106

Abstract of Dissertation Presented to the Graduate School
of the University of Florida in Partial Fulfillment of the
Requirements for the Degree of Doctor of Philosophy

A TIME-DEPENDENT MANY-ELECTRON APPROACH
TO ATOMIC AND MOLECULAR INTERACTIONS

By

KEITH RUNGE

May, 1993

Chairman: David A. Micha
Major Department: Physics

A new methodology is developed for the description of electronic rearrangement in atomic and molecular collisions. Using the eikonal representation of the total wavefunction, time-dependent equations are derived for the electronic densities within the time-dependent Hartree-Fock approximation. An averaged effective potential which ensures time reversal invariance is used to describe the effect of the fast electronic transitions on the slower nuclear motions. Electron translation factors (ETF) are introduced to eliminate spurious asymptotic couplings, and a local ETF is incorporated into a basis of traveling atomic orbitals. A reference density is used to describe local electronic relaxation and to account for the time propagation of fast and slow motions, and is shown to lead to an efficient

integration scheme. Expressions for time-dependent electronic populations and polarization parameters are given. Electronic integrals over Gaussians including ETFs are derived to extend electronic state calculations to dynamical phenomena.

Results of the method are in good agreement with experimental data for charge transfer integral cross sections over a projectile energy range of three orders of magnitude in the proton-Hydrogen atom system. The more demanding calculations of integral alignment, state-to-state integral cross sections, and differential cross sections are found to agree well with experimental data provided care is taken to include ETFs in the calculation of electronic integrals and to choose the appropriate effective potential. The method is found to be in good agreement with experimental data for the calculation of charge transfer integral cross sections and state-to-state integral cross sections in the one-electron heteronuclear Helium(2+)-Hydrogen atom system and in the two-electron system, Hydrogen atom-Hydrogen atom.

Time-dependent electronic populations are seen to oscillate rapidly in the midst of collision event. In particular, multiple exchanges of the electron are seen to occur in the proton-Hydrogen atom system at low collision energies. The concepts and results derived from the approach provide new insight into the dynamics of nuclear screening and electronic rearrangement in atomic collisions.

CHAPTER 1 INTRODUCTION

Electronic rearrangement in ionic, atomic, and molecular collisions is a subject of wide interdisciplinary interest. It deals with the basic concepts and methodology required in studies ranging from detailed atom-atom collision phenomena to phenomena in very complex systems. For example, electron transfer in photoexcited proteins and protein-enzyme interaction is of current interest in biological and biochemical research. Electron transfer in atom-surface and molecule-surface interaction is an area of active research in material science and electron transfer in electrochemical cells is of interest in current chemical engineering research. Thus, it is of far reaching importance to gain a fundamental understanding of the most basic time-dependent aspects of electron transfer phenomena in simple systems where detailed studies can be carried out. This thesis investigates these time-dependent phenomena in terms of a formalism developed to consider many active electrons.

Overview of Theoretical Methods

While the formalism developed is applicable to system involving many atomic cores and electrons, in this thesis we consider the most basic of collision in which there are only two cores and one or two active electrons. The earliest theoretical

treatment considered in this thesis is the Perturbed Stationary States treatment which dealt specifically with two identical cores and only one electron [1, 2]. Others have returned to this formalism more recently [3, 4]. In this treatment the two cores are taken to be essentially at rest with the motion of the cores taken to be a perturbation which induces electronic transitions. For example, the total wave function of the system with identical nuclei is written

$$\Psi(\vec{r}, \vec{R}) = X^+(\vec{r}, \vec{R})F^+(\vec{R}) + X^-(\vec{r}, \vec{R})F^-(\vec{R}) \quad (1.1)$$

where \vec{r} is the electron coordinate, \vec{R} is the intercore separation and $X^+(\vec{r}, \vec{R})$ and $X^-(\vec{r}, \vec{R})$ are symmetric and antisymmetric in the nuclear coordinates with coefficients $F^+(\vec{R})$ and $F^-(\vec{R})$, respectively. The total wave function is substituted into the time-dependent Schrödinger equation and the solutions are required to have this asymptotic form

$$F^\pm(\vec{R}) \sim \frac{1}{\sqrt{2}} [\exp(ik\hat{n} \cdot \vec{R}) + R^{-1}f^\pm(\Theta) \exp(ikR)] \quad (1.2)$$

where k is the magnitude of the initial wave vector of the relative motion, \hat{n} is a unit vector in the direction of the final relative motion, Θ is the scattering angle and $f^\pm(\Theta)$ are the scattering amplitudes. The integral charge transfer cross section is then expressed as

$$\sigma = \frac{1}{4} \int_0^{2\pi} \int_0^\pi [f^+ - f^-]^2 \sin \Theta d\Theta d\Phi \quad (1.3)$$

While this theory obtains good results for integral cross sections at low energies, its assumption breaks down at higher energies and the inclusion of more than two total states for the wave function complicates the theory. Perturbed stationary states also fail to give time dependent information about the collision.

Another approach to the dynamics of collisional systems has been the direct numerical integration of the Schrödinger equation within the impact parameter approximation [5]. In this reference, the collision system has been assumed to be homonuclear and occurs in the x-z plane. The time-dependent Schrödinger equation is then written in cylindrical coordinates as

$$i\partial\psi(\rho, z, \varphi, t)/\partial t = [-\frac{1}{2}\nabla^2 + V(\rho, z, t) - \frac{d\theta}{dt}L_y]\psi(\rho, z, \varphi, t) \quad (1.4)$$

where $\psi(\rho, z, \varphi, t)$ is the electronic wave function, L_y is the y-component of the angular momentum operator, θ is the angle of rotation between the space-fixed and body-fixed axes in the x-z plane, and the Coulomb potential V is given by

$$V(\rho, z, t) = -\{\rho^2 + [z + \frac{1}{2}R(t)]^2\}^{-\frac{1}{2}} - \{\rho^2 + [z - \frac{1}{2}R(t)]^2\}^{-\frac{1}{2}} \quad (1.5)$$

where $R(t)$ is the internuclear separation. Expansion of the wave function in the eigenfunctions of the z component of the angular momentum reduces the problem to one of two spatial variables. After the initial wave function is specified on a grid in the ρ -z plane, the numerical integration is carried out. In this reference, the nuclear trajectory is assumed to be a straight line with constant velocity. While this method can give electronic densities as a function of time, it does not give

insight into other physical properties. The restriction of straight line trajectories hinders the determination of differential cross sections and integral cross sections at low collision energies. At higher collision energies, the method gives good total integral cross sections and state-to-state integral cross sections. Finally, the method is very computationally intensive so that generalizing it to larger systems may not be practical.

By far the most popular method for calculating the dynamic of collisional system is that of close-coupling. Two recent reviews give a good overview of this work [6, 7]. In this method, the time dependent electronic wave function is expanded in a basis of atomic states, molecular states, pseudo-states, or a combination of such states

$$\Psi(\vec{r}, t) = \sum_{k=1}^N a_k(t) \psi_k(\vec{r}, t) \quad (1.6)$$

where the expansion coefficients $a_k(t)$ are complex and time dependent. The expansion coefficients are propagated through time using the time-dependent Schrödinger equation along a chosen nuclear trajectory. In these calculations the trajectory choice is generally the straight line trajectory with constant velocity. After the completion of the nuclear trajectory the transition probability to a final state f is given by

$$P_{i \rightarrow f}(v, b) = |a_f(+\infty)|^2 \quad (1.7)$$

where b is the impact parameter and the state-to-state integral cross section to this state is

$$\sigma_{i \rightarrow f}(v) = 2\pi \int_0^{\infty} b P_{i \rightarrow f}(v, b) db \quad (1.8)$$

The choice of basis functions is what distinguishes the various close-coupled calculations.

The earliest choice of basis functions was the hydrogenic functions [8–10]. All of these studies included electron translation factors and hydrogenic orbitals on each center. The role of electron translation factors will be discussed in chapter 3. Various types of atomic orbitals have been used in calculations involving two centers. Some of these consider atomic orbitals appropriate to the individual centers only and are called AO approaches [11–13]. Others include not only atomic orbitals appropriate to the individual centers but also those appropriate to the charge of the united atom. These are called AO+ approaches [14–16]. Another common choice of basis functions is a set of molecular orbitals [17–20]. It is more difficult to decide the proper choice of the electron translation factor in this basis. It is also necessary to match the molecular orbital basis to an atomic orbital basis asymptotically to obtain cross section information. Pseudo-states have been included in the expansion of atomic orbitals including Sturmians and Hylleraas functions [21–23]. Finally, there has been an attempt at improving upon the trajectory choice through the so-called common trajectory method [24, 25].

While close-coupled calculations give good agreement with experimental results at high energies, the generalization of this method to more than two centers is quite challenging. Also the calculation of time dependent quantities of physical interest has not been done within the close-coupled method.

The present method combines and builds upon methods developed over a number of years using eikonal procedures and time-dependent Hartree-Fock states [26–30]. The eikonal representation of the total wave function of a system and its relationship to the eikonal approximation have been developed particularly in the context of fast and slow degrees of freedom. Time-dependent Hartree-Fock has been the subject of much investigation particularly into the circumstances in which time-dependent Hartree-Fock must be improved. A general variational method based on a transition functional has provided an improvement scheme and has been applied to the Helium(2+)-Helium collisional system [31]. The development of the present method was initially concerned with the equations for the time propagation of the electronic densities within time-dependent Hartree-Fock theory and with the coupling of electronic and nuclear motions [32–34]. In this method, we use the equations for the time propagation of the electronic density operator

$$i\frac{\partial \hat{\rho}}{\partial t} = \hat{F}\hat{\rho} - \hat{\rho}\hat{F} \quad (1.9)$$

where $\hat{\rho}$ is the electronic density operator and \hat{F} is the Fock operator. The

choice of propagating the electronic densities is motivated by the fact that the electronic density is more fundamental to the physics of collisional systems than the expansion of the wave function in molecular orbitals. The electronic density also has the advantage of being closely related to physical quantities. The method has been further developed to consider such physical quantities as the time-evolution of electronic polarization and electronic populations and to calculate collisional polarization parameters [35, 36].

An approach of interest related to this thesis is based on the time-dependent variational principle and coherent states [37, 38]. It has recently been applied to the electron-nuclear dynamics of atom-atom collisions [39]. This theory is allied to the present method in that it is also a time-dependent Hartree-Fock method in which the nuclear and electronic degrees of freedom are coupled. The formalism is developed in a coherent states representation so that wave function takes the form

$$|z\rangle = \exp\left(\sum_{p,h} z_{ph} b_p^\dagger b_h\right) |0\rangle \quad (1.10)$$

where $|0\rangle$ is a single-determinantal reference wave function, b_p^\dagger and b_h are the creation and annihilation operators, respectively, and the complex parameters z_{ph} called the Thouless parameters define the state of the system. The time-dependent Hartree-Fock equations are derived as a special case of a more general time-dependent variational principle and the Thouless parameters are propagated

through time. The coupling of the nuclear and electronic motion is accomplished through the use of a time reversal invariant generalization of the Ehrenfest potential to account for the effect of the electronic motion on the nuclear motion.

Outline of the Thesis

Chapter 2 deals with the coupling of electronic and nuclear degrees of freedom within the eikonal representation. The electronic degrees of freedom are treated quantally and the potential the cores experience due to the electrons is formulated in a time reversal invariant form. Definitions of the types of electronic potentials used throughout the thesis are given. Chapter 3 presents the derivation of the time-dependent Hartree-Fock equations for the electronic density matrices. The derivation includes a detailed exposition of the formal role of the electron translation factor in the context of the present approach. Chapter 4 develops a method for the solution of these equations by a temporal linearization technique. A solution of the linearized equations by an exponential expansion is presented, and practical criteria for the efficient integration of the equations are advanced. Chapter 5 discusses time-dependent properties for the more detailed description of collisional dynamics. Particular attention is given to measures of electronic population and polarization parameters.

Chapter 6 sets out the procedure for the integration of the linearized time-dependent Hartree-Fock equations along with the integration of the nuclear

equations of motion. A scheme is developed which allows for the rapid integration of these equations without a loss of accuracy. Chapter 7 deals with our basis set choices and their effects on our calculations. The role of electron translation factors at differing core velocities is considered. A method for the inclusion of electron translation factors in overlap and Hamiltonian integrals involving two centers is developed for Gaussian-type orbitals.

Chapter 8 discusses the results of the application of our method to the proton-Hydrogen collisional systems. Results are presented over a range of projectile energies from a few eV to a few keV for charge transfer integral cross section, state-to-state integral cross sections, differential cross sections, and integral alignment. Time evolution of electronic populations and alignment parameters is also presented. Chapter 9 contains results for charge transfer integral cross section and state-to-state integral cross sections for the Helium(2+)-Hydrogen collisional system. Again, time evolution of electronic populations and alignment parameters are shown. Chapter 10 considers the two active electron Hydrogen-Hydrogen collisional system. Integral state-to-state cross sections and time evolution of electronic populations are presented. Chapter 11 discusses the method and describes possible improvement to the methods and future directions. Appendices A and B present the details of the calculation of overlap and Hamiltonian matrix

elements in the Hydrogenic and travelling Gaussian bases, respectively. Appendix C presents a flow diagram of the time-dependent density matrix code.

CHAPTER 2

COUPLING OF ELECTRONIC AND NUCLEAR MOTIONS

The Hamiltonian operator and the total wavefunction of a collisional system can be written in atomic units as

$$\hat{H} = -\frac{1}{2M} \frac{\partial^2}{\partial \mathbf{R}^2} + \hat{H}_{\mathbf{R}}\left(\frac{\partial}{\partial \mathbf{X}}, \mathbf{X}\right) \quad (2.1)$$

$$\Psi(\mathbf{X}, \mathbf{R}) = \chi(\mathbf{X}, \mathbf{R}) \exp[iS(\mathbf{R})]$$

where \mathbf{X} and \mathbf{R} are the active electronic and core coordinates. The second term in the Hamiltonian describes the active electronic system for fixed cores. The function S is real, while χ is complex-valued; in our treatment we choose S for convenience to be an action integral approximating the quantal phase of the wavefunction; the phase of χ can compensate in principle for deviations from the correct phase. We refer to this decomposition of the wavefunction as the eikonal representation.

For total energy E , we place the wavefunction in the time-independent Schrödinger equation to obtain

$$[\frac{1}{2M}(-i\frac{\partial}{\partial \mathbf{R}} + \frac{\partial S}{\partial \mathbf{R}})^2 + \hat{H}_{\mathbf{R}} - E]\chi(\mathbf{R}) = 0 \quad (2.2)$$

which is valid for any S . A specific equation for S follows by projecting equation 2.2 on χ , and taking the real part of the result, which gives [26, 29]

$$\begin{aligned} \frac{1}{2M}(\frac{\partial S}{\partial \mathbf{R}})^2 + V_{qu}(\frac{\partial S}{\partial \mathbf{R}}, \mathbf{R}) &= E \\ V_{qu} &= \langle \chi(\mathbf{R}) | \hat{H}_{\mathbf{R}} | \chi(\mathbf{R}) \rangle / \langle \chi(\mathbf{R}) | \chi(\mathbf{R}) \rangle + V^{(1)} + V^{(2)} \end{aligned} \quad (2.3)$$

where $V^{(1)}$ and $V^{(2)}$ contain $\partial\chi/\partial\mathbf{R}$ and $\partial^2\chi/\partial\mathbf{R}^2$ respectively, and the first term can be identified as the Ehrenfest potential for the core motions.

Defining the momentum

$$\mathbf{P}_R = \partial S / \partial \mathbf{R} \quad (2.4)$$

trajectories of the cores follow, introducing the time t , from

$$\begin{aligned} H_{qu} &= \mathbf{P}_R \cdot \dot{\mathbf{P}}_R / (2M) + V_{qu}(\mathbf{P}_R, \mathbf{R}) \\ d\mathbf{R}/dt &= \partial H_{qu} / \partial \mathbf{P}_R \\ d\mathbf{P}_R/dt &= -\partial H_{qu} / \partial \mathbf{R} \end{aligned} \quad (2.5)$$

for initial $(\mathbf{P}_{R_a}, \mathbf{R}_a)$ and give

$$S(\mathbf{R}) = S(\mathbf{R}_a) + \int_{\mathbf{R}_a}^{\mathbf{R}} d\mathbf{R} \cdot \dot{\mathbf{P}}_R \quad (2.6)$$

We assume in this treatment that the electronic states can be obtained from the time-dependent Hartree-Fock (TDHF) approximation. This includes electron correlation (beyond the time-independent HF approximation), and electronically diabatic effects, insofar as it allows for electronic transitions induced by the core motions. We further assume that we can obtain the effective potential within an eikonal (short wavelength) approximation. We, therefore, neglect $V^{(1)}$ and $V^{(2)}$ in equation 2.3 and write the effective potential

$$V_{qu} = \text{tr}[\hat{\rho} \frac{(\hat{F} + \hat{H}_c)}{2}] \quad (2.7)$$

however, as the Fock operator, \hat{F} , the core Hamiltonian \hat{H}_c and the density operator $\hat{\rho}$ are each functions of time, this Ehrenfest potential is neither manifestly nor generally time reversal invariant for state-to-state transitions. An averaged effective electronic potential can be written in a form invariant under time reversal

$$V_{qu} = \sum_{\mu} \text{tr}[\hat{\rho}_{\mu} \frac{(\hat{F} + \hat{H}_c)}{2}] w_{\mu} \quad (2.8)$$

where μ denotes the initial electronic state of the system and the w_{μ} are appropriately chosen weights. This potential will be time reversal invariant if all the appropriate active channels are considered. Criteria for the choice of appropriate weight functions include

1. All open channels in the case where only open channels participate in a given collision.
2. All resonant virtual excitation channels which predominate in a given collision.

In this work we have employed a number of approximate potentials for the motions of the cores. The first approximation, known as the Impact Parameter Approximation, consists of allowing the core-core potential and the core-electron potential to be zero (ZP). The result is a rectilinear trajectory for the cores with constant velocity. This approximation is best used at high collision energies and is used for the purpose of comparison to other results in the literature.

A second approximate potential we will employ we call the Coulomb Potential (CP). It consists of keeping the core repulsion while setting the core-electron potential to zero.

$$V = V_{\text{core}} = \zeta_A \zeta_B / R_{AB} \quad (2.9)$$

Here ζ_N is the effective charge on center N. This approximation will be used to compare with the Impact Parameter Approximation and other more exact forms for the core-electron potential. One would expect that the Coulomb potential would be most successful at fairly high collision energies.

A third approximate potential we will call the Screened Coulomb Potential (SCP). This choice of potential consists of keeping the core repulsion while choosing the weights w_μ from equation 2.8 such that the core screening by the valence electrons for the ground states in a given system is included while all other electronic states are ignored. This potential is especially successful when lower collision energies are involved and particularly for low collision energy, resonant transfer phenomena. It will be shown to give results in good agreement with sensitive experimental quantities such as differential cross sections.

A fourth approximate potential will be the Averaged Effective Potential (AEP). This choice of potential involves retaining the core repulsion while choosing weights w_μ from equation 2.8 such that all open channels for a given collision are

equally weighted. This potential should be successful at intermediate and lower collision energies and particularly for nonresonant transfer collisional phenomena.

CHAPTER 3

THE TIME-DEPENDENT HARTREE-FOCK EQUATIONS

The inclusion of time dependence in the theory of ionic, atomic, and molecular collisions entails a number of challenges. Unlike the time-independent theory, time-dependent Hartree-Fock needs to consider a large range of core geometries and nonequilibrium electronic configurations. Further the integration of the time-dependent Hartree-Fock equations must allow for rapid variations in electronic densities around a given core. It would also be helpful if these equations offered a unique physical insight into the dynamics of collisional systems involving both fast and slow degrees of freedom.

A collisional system including ions, atoms, and molecules will be characterized by a mathematical description of the core and electronic degrees of freedom. In the present method the core degrees of freedom will be treated classically (see Chapter 2). The electronic degrees of freedom will be described quantally through the time-dependent Hartree-Fock equation. One further needs to decide whether one wishes to treat the electronic degrees of freedom by the propagation of their wave function through time or an alternative quantity. In the present method we opt to propagate the electronic density matrices through time as opposed to propagating the electronic wave function or some other amplitude.

The time-dependent Hartree-Fock equations for the electronic densities can be written in operator notation with $\hbar = 1$,

$$i\dot{\hat{\rho}}^\gamma = \hat{F}^\gamma \hat{\rho}^\gamma - \hat{\rho}^\gamma \hat{F}^\gamma \quad (3.1)$$

where the dot denotes differentiation with respect to time,

$$\hat{\rho}^\gamma = \sum_{\text{occ } i} |\phi_i^\gamma\rangle\langle\phi_i^\gamma| \quad (3.2)$$

is the electronic density operator for electron spin γ and ϕ_i^γ are the molecular orbitals which compose the time-dependent Hartree-Fock state, and the Fock operator is defined by

$$\hat{F}^\gamma = \hat{H}_c + \hat{G}^\gamma[\hat{\rho}^\gamma, \hat{\rho}^{\gamma'}] \quad (3.3)$$

with the single electron Hamiltonian \hat{H}_c , and the electron-electron interaction \hat{G}^γ .

We expand the molecular orbitals as linear combinations of traveling atomic orbitals (TAOs). We implement this expansion by writing the molecular orbitals

$$\phi_i^\gamma(\vec{r}_j, t) = \sum_\mu T_m(\vec{r}_j, t) \chi_\mu(\vec{r}_{mj}) c_{\mu i}^\gamma(t) \quad (3.4)$$

Here we have introduced the local version of the electron translation factor (ETF) [40, 41]

$$T_m(\vec{r}_j, t) = \exp[i m_e (\vec{v}_m \cdot \vec{r}_j - \frac{1}{2} \int_{t_0}^t v_m^2 dt')] \quad (3.5)$$

where the local velocity vector for core m is \vec{v}_m , the position of the jth electron with respect to a space-fixed origin is \vec{r}_j , the position of the jth electron with respect to core m is \vec{r}_{mj} , the mass of the electron is m_e , an atomic orbital centered at m is χ_μ , and the expansion coefficients are $c_{\mu i}^\gamma$. The role of the electron translation factor is to cancel spurious couplings that arise from the kinetic energy operator acting on atomic states whose origins are functions of time. Here we will consider only situations in which the asymptotic accelerations of the cores are zero. This construction can be modified to include asymptotically accelerating particles. The single-electron Hamiltonian can be written as a sum of kinetic and potential energy operators

$$\hat{H} = \hat{T} + \hat{V} \quad (3.6)$$

where the kinetic energy operator is defined by

$$\hat{T} = -\frac{1}{2m_e} \sum_j \nabla_{\vec{r}_j}^2 \quad (3.7)$$

Consider the action of the time derivative on an atomic state with an origin that is a function of time in the asymptotic region.

$$i\left(\frac{\partial}{\partial t}\right)_{\{\vec{r}_j\}} \chi_\mu(\vec{r}_{mj}) = i\left[\left(\frac{\partial}{\partial t}\right)_{\{\vec{R}_m\}} + \frac{d\vec{R}_m}{dt} \cdot \nabla_{\vec{R}_m}\right] \chi_\mu(\vec{r}_{mj}) \quad (3.8)$$

where the brackets indicate which quantities are held constant while the partial time derivative is taken. Note the presence of the gradient with respect to the core coordinate \vec{R}_m on the right hand side of equation 3.3. This is often referred to

as the spurious gradient coupling which causes the mixing of pure atomic states on the core m . Introducing the TAO

$$\xi_\mu(\vec{r}_j, t) = T_m(\vec{r}_j, t)\chi_\mu(\vec{r}_{mj}) \quad (3.9)$$

applying the time derivative operator to a TAO we obtain

$$\begin{aligned} i\left(\frac{\partial}{\partial t}\right)_{\{\vec{r}_j\}} \xi_\mu(\vec{r}_j, t) &= i\left[\left(\frac{\partial}{\partial t}\right)_{\{\vec{R}_m\}} + \frac{d\vec{R}_m}{dt} \cdot \nabla_{\vec{R}_m}\right] \xi_\mu(\vec{r}_j, t) \\ &= i\left[\left(\frac{\partial}{\partial t}\right)_{\{\vec{R}_m\}} + \vec{v}_m \cdot \nabla_{\vec{R}_m}\right] \xi_\mu(\vec{r}_j, t) \end{aligned} \quad (3.10)$$

where we employ the fact that \vec{r}_j is independent of time. Continuing in more detail

$$\begin{aligned} i\left(\frac{\partial}{\partial t}\right)_{\{\vec{r}_j\}} |T_m \chi_\mu\rangle &= \frac{m_e |\vec{v}_m|^2}{2} T_m |\chi_\mu\rangle + iT_m \left(\frac{\partial}{\partial t}\right)_{\{\vec{R}_m\}} |\chi_\mu\rangle \\ &\quad + iT_m \vec{v}_m \cdot \nabla_{\vec{R}_m} |\chi_\mu\rangle \\ \hat{T} |T_m \chi_\mu\rangle &= \left[\frac{m_e |\vec{v}_m|^2}{2} T_m - i\vec{v}_m \cdot \nabla_{\vec{r}_j} + T_m \hat{T} \right] |\chi_\mu\rangle = \\ &\quad \left[\frac{m_e |\vec{v}_m|^2}{2} T_m + iT_m \vec{v}_m \cdot \nabla_{\vec{R}_m} + T_m \hat{T} \right] |\chi_\mu\rangle \end{aligned} \quad (3.11)$$

Here one can readily see that in the limit where the acceleration can be neglected the first and third terms from the time derivative cancel the first and second term in the kinetic energy, respectively. This leaves the usual time-dependent Hartree-Fock equation in the ξ -basis, but with an altered kinetic energy operator

$$\hat{T}_T |\xi_\mu\rangle = T_m \hat{T} T_m^{-1} |\xi_\mu\rangle \quad (3.12)$$

Hence, the modified Fock-like operator can be defined by

$$\hat{F}_T |\xi_\mu\rangle = T_m \hat{F} T_m^{-1} |\xi_\mu\rangle \quad (3.13)$$

which is not generally a Hermitian operator. We may now write the time-dependent Hartree-Fock equation in the TAO basis

$$\begin{aligned} \mathbf{F}_T^\gamma \mathbf{P}^\gamma - \mathbf{P}^\gamma \mathbf{F}_T^{\gamma\dagger} &= i\mathbf{S}\dot{\mathbf{P}}^\gamma\mathbf{S}^\gamma \\ \mathbf{S}^{-1}\mathbf{F}_T^\gamma \mathbf{P}^\gamma - \mathbf{P}^\gamma \mathbf{F}_T^{\gamma\dagger} \mathbf{S}^{-1} &= i\dot{\mathbf{P}}^\gamma \end{aligned} \quad (3.14)$$

where bold type indicates matrices in the TAO basis, \mathbf{S}^{-1} is the inverse of the overlap matrix, \mathbf{F}_T^γ is the modified Fock-like matrix and the density matrix is given by its usual definition in terms of the expansion coefficients

$$P_{\mu\nu}^\gamma(t) = \sum_{occ\ i} c_{\mu i}^\gamma(t) c_{\nu i}^\gamma(t)^* \quad (3.15)$$

In the next chapter we will present a method of solution of these equations for the propagation of the electronic density by the method of temporal linearization.

CHAPTER 4
TEMPORAL LINEARIZATION OF THE
TIME-DEPENDENT HARTREE-FOCK EQUATIONS

In the previous chapter, we derived the Hartree-Fock equations for the electronic densities in matrix form for a basis of traveling atomic orbitals. In this chapter we will present a method for solution of these equations employing the technique of temporal linearization. The linearization procedure can be presented in operator notation. Let us begin by writing the electronic density operator in the time interval between t_0 and t as

$$\hat{\rho}^\gamma(t) = \hat{\rho}^{(0)\gamma}(t) + \sigma^\gamma(t) \quad (4.1)$$

Further define the reference density $\hat{\rho}^{(0)\gamma}$ to satisfy the equation

$$i\dot{\hat{\rho}}^{(0)\gamma}(t) = \hat{F}_T^\gamma(t_0)\hat{\rho}^{(0)\gamma}(t) - \hat{\rho}^{(0)\gamma}(t)\hat{F}_T^\gamma(t_0)^\dagger \quad (4.2)$$

Here we need to make some remarks concerning the modified Fock-like operator which can be written

$$\hat{F}_T^\gamma[\hat{\rho}^\gamma, \hat{\rho}^{\gamma'}] = \hat{T}_T + \hat{V}_c + \hat{G}[\hat{\rho}^\gamma, \hat{\rho}^{\gamma'}] \quad (4.3)$$

where \hat{T}_T is the modified kinetic energy term, \hat{V}_c is the core potential, and $\hat{G}[\hat{\rho}^\gamma, \hat{\rho}^{\gamma'}]$ is the electron-electron interactions among active electrons. The choice of core potential and definition of active electrons will vary from system to system and will also depend on the collision energies to be considered.

Given these definitions, we can then derive an equation for the change in the density matrix $\hat{\sigma}^\gamma(t)$ and keep terms only to first order in this change in the density matrix.

$$\begin{aligned} i\dot{\hat{\sigma}}^\gamma(t) &= \hat{F}_T^\gamma(t_0)\hat{\sigma}^\gamma(t) - \hat{\sigma}^\gamma(t)\hat{F}_T^\gamma(t_0)^\dagger + \\ &\Delta\hat{H}_T^c(t)\hat{\rho}^{(0)\gamma}(t) - \hat{\rho}^{(0)\gamma}(t)\Delta\hat{H}_T^c(t)^\dagger + \\ &\Delta\hat{G}[\hat{\rho}^{(0)\gamma}, \hat{\rho}^{(0)\gamma'}]\hat{\rho}^{(0)\gamma}(t) - \hat{\rho}^{(0)\gamma}(t)\Delta\hat{G}[\hat{\rho}^{(0)\gamma}, \hat{\rho}^{(0)\gamma'}] \end{aligned} \quad (4.4)$$

where

$$\begin{aligned} \Delta\hat{H}_T^c(t) &= \hat{T}_T(t) + \hat{V}_c(t) - [\hat{T}_T(t_0) + \hat{V}_c(t_0)] \\ \Delta\hat{G}[\hat{\rho}^{(0)\gamma}, \hat{\rho}^{(0)\gamma'}] &= \hat{G}[\hat{\rho}^{(0)\gamma}(t), \hat{\rho}^{(0)\gamma'}(t)] - \hat{G}[\hat{\rho}^{(0)\gamma}(t_0), \hat{\rho}^{(0)\gamma'}(t_0)] \end{aligned} \quad (4.5)$$

We can now see that the reference density that we have defined has the effect of separating the electronic density's evolution arising from the TDHF equation with the cores fixed, from the electronic density's evolution that arises from the effect of the movement of the cores. More specifically the reference density $\hat{\rho}^{(0)\gamma}$ evolves as though the cores are fixed while the change in the density $\hat{\sigma}^\gamma(t)$ corrects for the effect of the movement of the cores.

These equations move easily into the TAO basis matrix form, with equation 4.2 for the reference density becoming

$$i\dot{\mathbf{P}}^{(0)\gamma}(t) = \mathbf{W}^\gamma(t_0)\mathbf{P}^{(0)\gamma}(t) - \mathbf{P}^{(0)\gamma}(t)\mathbf{W}^\gamma(t_0)^\dagger \quad (4.6)$$

where

$$\mathbf{W}^\gamma = \mathbf{S}^{-1}\mathbf{F}_T^\gamma \quad (4.7)$$

Continuing along this path, equations 4.4 and 4.5 for the change of the density may be written in matrix form

$$\begin{aligned} i\dot{\mathbf{Q}}^\gamma(t) &= \mathbf{W}^\gamma(t_0)\mathbf{Q}^\gamma(t) - \mathbf{Q}^\gamma(t)\mathbf{W}^\gamma(t_0)^\dagger + \mathbf{D}^\gamma(t) \\ \mathbf{D}^\gamma(t) &= \Delta\mathbf{W}^{(0)\gamma}(t)\mathbf{P}^{(0)\gamma}(t) - \mathbf{P}^{(0)\gamma}(t)\Delta\mathbf{W}^{(0)\gamma}(t)^\dagger \end{aligned} \quad (4.8)$$

where in the driving term $\mathbf{D}^\gamma(t)$ we define

$$\mathbf{W}^{(0)\gamma} = \mathbf{S}^{-1}\left(\mathbf{H}^c + \mathbf{G}[\mathbf{P}^{(0)\gamma}, \mathbf{P}^{(0)\gamma'}]\right) \quad (4.9)$$

The matrix equations for the electronic densities are a set of linear first-order differential equations. The solution to these equations is problematic as the change in the density, as well as the reference density, may oscillate significantly. Therefore, we choose to solve these equations using an exponential expansion. In this procedure, the change in the density matrix is expressed as

$$\mathbf{Q}^\gamma(t) = \exp(-i\mathbf{W}^\gamma t)\mathbf{Q}'(t)\exp(i\mathbf{W}^{\gamma\dagger} t) \quad (4.10)$$

Substituting equation 4.10 into equation 4.8, we obtain

$$i\exp(-i\mathbf{W}^\gamma t)\dot{\mathbf{Q}}'(t)\exp(i\mathbf{W}^{\gamma\dagger} t) = \mathbf{D}^\gamma(t) \quad (4.11)$$

Returning to $\mathbf{Q}^\gamma(t)$, its expression at time t_1 is

$$\begin{aligned} \mathbf{Q}^\gamma(t_1) &= -i\exp(-i\mathbf{W}^\gamma t_1) \times \\ &\left[\int_{t_0}^{t_1} \exp(i\mathbf{W}^\gamma t') \mathbf{D}^\gamma(t') \exp(-i\mathbf{W}^{\gamma\dagger} t') dt' \right] \exp(i\mathbf{W}^{\gamma\dagger} t_1) \end{aligned} \quad (4.12)$$

Introducing the biorthogonal transformations which diagonalize \mathbf{W}^γ and $\mathbf{W}^{\gamma\dagger}$

[42]

$$\begin{aligned}\mathbf{W}^\gamma &= \mathbf{L} \mathbf{w}^\gamma \bar{\mathbf{L}}^\dagger \\ \mathbf{W}^{\gamma\dagger} &= \bar{\mathbf{L}} \mathbf{w}^\gamma \mathbf{L}^\dagger\end{aligned}\quad (4.13)$$

We may now write the matrix elements of the change of the density

$$Q_{\mu\nu}^\gamma(t_1) = -i \sum_{j\rho\sigma k} L_{\mu j} \bar{L}_{j\rho}^\dagger \Gamma_{j\rho\sigma k}^\gamma \bar{L}_{\sigma k} \bar{L}_{k\nu}^\dagger \quad (4.14)$$

where

$$\Gamma_{j\rho\sigma k}^\gamma(t_1, t_0) = \int_{t_0}^{t_1} \exp[-i(w_j^\gamma - w_k^{\gamma*})(t_1 - t')] D_{\rho\sigma}^\gamma(t') dt' \quad (4.15)$$

where the w_j^γ are complex eigenvalues of the matrix \mathbf{W}^γ . Hence, we have replaced the single integral over time, from the initial time to the final time, by a series of integrations from t_0 to t_1 where t_0 is the initial time and t_1 is the final time corresponding to the chosen ending separation between the cores. The advantage of such an approach is that the problem of rapid variations in the density matrix is avoided by accounting for such variations explicitly in the diagonalization of the \mathbf{W}^γ and $\mathbf{W}^{\gamma\dagger}$ matrices.

In the case of two or more active electrons a tolerance for iterative solution of the TDHF equations will be considered. If the ratio of the magnitude of the change of the density matrix to the magnitude of the density matrix itself is greater than a given tolerance

$$\epsilon_{iter} < \frac{||\mathbf{Q}^\gamma(t_1)||}{||\mathbf{P}^\gamma(t_1)||} \quad (4.16)$$

we return to time t_0 substituting

$$\begin{aligned} \mathbf{P}_{n+1}^{\gamma}(t_0) &= \mathbf{P}_n^{\gamma}(t_0) + f \mathbf{Q}_n^{\gamma}(t_1) \\ 0 \leq f \leq 1 \end{aligned} \quad (4.17)$$

where the subscript indicates the number of iterations, to define a new starting point for the reference density. The choice of the fractional weight f is made to optimize the convergence of the iterative procedure. The procedure can be portrayed schematically

$$\begin{aligned} (\mathbf{P}^{(0)\gamma}, \mathbf{Q}^{\gamma})_{old} \rightarrow if \epsilon_{iter} < \frac{||\mathbf{Q}^{\gamma}(t_1)||}{||\mathbf{P}^{\gamma}(t_1)||} \rightarrow \mathbf{P}_{new}^{\gamma}(t_0) &= \mathbf{P}_{old}^{\gamma}(t_0) + f \mathbf{Q}_{old}^{\gamma}(t_1) \\ \rightarrow else \ accept \end{aligned} \quad (4.18)$$

Here the first line is repeated until the iteration criterion is satisfied.

The above separation of the density matrix into a reference density and a change in the density matrix leads naturally to a set of criteria for the appropriate choice of t_0 and t_1 . A time step

$$\Delta t = t_1 - t_0 \quad (4.19)$$

will be deemed acceptable provided the ratio of the magnitude of the change of the density matrix to the magnitude of the density matrix itself is between given tolerances,

$$\epsilon_{lower} < \frac{||\mathbf{Q}^{\gamma}(t_1)||}{||\mathbf{P}^{\gamma}(t_1)||} < \epsilon_{higher} \quad (4.20)$$

Here the lower tolerance ϵ_{lower} allows the method to take larger time steps in any region in which the evolution of the density matrix is essentially equal to

the evolution of the reference density. The higher tolerance ϵ_{higher} restricts the method to take smaller time steps in any region in which the change in the density matrix is of great importance, thereby keeping the error in the procedure within a prescribed level. The present method is therefore able to automatically adjust its time step size in order to maximize the performance of the method in terms of taking the minimum number of possible steps for the maximum accuracy for those steps. In practice the choice of tolerances will be shown to be rather flexible in achieving the desired accuracy in an acceptable amount of computing time.

In the case of one active electron, we simply replace the Fock operator with the full Hamiltonian for the active electron. So we write, for a given spin,

$$\mathbf{W} = \mathbf{S}^{-1} \mathbf{H}_T \quad (4.21)$$

the remainder of the development proceeds as above. There is no need for iterative propagation in the one active electron limit. This method will be used to investigate electron transfer and excitation in systems with one active electron. We will use this method to investigate polarization and alignment effects in collisions. The effect of electron translation factors and differing basis sets will be investigated. We will also explore candidates for the description of time-dependent phenomena during atom-atom and atom-ion collisions which will serve as the topic of the next chapter.

CHAPTER 5

TIME-DEPENDENT ELECTRONIC ALIGNMENT AND POPULATION ANALYSES

It is of interest to describe in some way what is occurring during collisional electronic excitation and rearrangement. Among the possible quantities of interest are the alignment and orientation parameters of the collisional system and the electronic populations of the atomic and molecular orbitals of the system. While a number of descriptions appropriate to time-independent calculations are available in the literature, we will propose a number of time-dependent extensions of some of these descriptions. We will evaluate these extension by applying them to a number of differing collisional systems for a variety of collision energies. Further, we will discuss the applicability of these measures of electronic alignment and population with particular emphasis on physical insights gained from time-dependent studies.

In this study, we will always consider the plane of the collision to be the x-z plane with the z-direction being the incoming direction of the projectile and the x-direction being the direction of the impact parameter, so that the y-direction is always perpendicular to the plane. A few other investigators choose the plane of the collision to be the x-y plane [43, 44], but the consensus of the field seems to agree with our calculational geometry [45, 46].

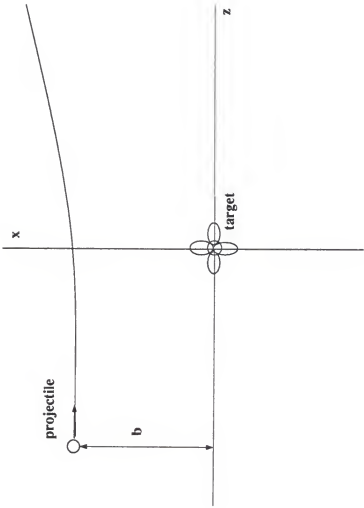


Figure 5-1: The collision is taken to occur in the x - z plane.

Having chosen this particular geometry, we may embark upon the definition of orientation and alignment parameters. In general one may describe the orbital polarization of a system by examining the anisotropy of the orbital angular momentum of the electrons. A state of given angular momentum L is said to be [47]

1. Isotropic, if all its magnetic substates are equally populated.
2. Oriented, if the magnetic substates have differing populations.
3. Aligned, if substates with magnetic quantum numbers of equal magnitude but opposite signs are equally populated.

To illustrate these definitions let us consider a system with total angular momentum \vec{J} . We may introduce the spherical irreducible tensor operators $\hat{J}_q^{(n)}$, where we will consider $n=1,2$ and $-n \leq q \leq n$

$$\begin{aligned}\hat{J}_0^{(1)} &= \hat{J}_z \\ \hat{J}_{\pm 1}^{(1)} &= \mp \frac{1}{\sqrt{2}} \hat{J}_{\pm} \\ \hat{J}_0^{(2)} &= \frac{1}{\sqrt{6}} (3\hat{J}_z^2 - \hat{J}^2) \\ \hat{J}_{\pm 1}^{(2)} &= \mp \frac{1}{2} \hat{J}_{\pm} (2\hat{J}_z \pm 1) \\ \hat{J}_{\pm 2}^{(2)} &= \frac{1}{2} \hat{J}_{\pm}^2\end{aligned}\tag{5.1}$$

where we define in Cartesian coordinates

$$\hat{J}_{\pm} = \hat{J}_x \pm i\hat{J}_y\tag{5.2}$$

The action of the operators is defined by

$$\begin{aligned} [\hat{J}_z, \hat{J}_q^{(k)}] &= q\hat{J}_q^{(k)} \\ [\hat{J}_{\pm}, \hat{J}_q^{(k)}] &= \sqrt{k(k+1) - q(q \pm 1)}\hat{J}_{q \pm 1}^{(k)} \end{aligned} \quad (5.3)$$

where the square brackets indicate the commutator. Let us now define the orientation vector $O_q^{(1)}$ and the alignment tensor $A_q^{(2)}$ at time t ,

$$O_q^{(1)}(J, t) = \frac{1}{\sqrt{J(J+1)}} \text{Re}\langle \hat{J}_q^{(1)} \rangle_t \quad (5.4)$$

$$A_q^{(2)}(J, t) = \frac{\sqrt{6}}{J(J+1)} \text{Re}\langle \hat{J}_q^{(2)} \rangle_t \quad (5.5)$$

where the angle brackets indicate the expectation value with respect to $\rho(t)$ for a given J . These quantities can be expressed in terms of the density matrices and hence may be calculated as functions of time in our method. Examining the expression for the expectation value of the spherical irreducible tensor operators we may write

$$\langle \hat{J}_q^{(n)} \rangle_m = \text{tr}[\hat{\rho}(\hat{J}_q^{(n)})_m] \quad (5.6)$$

where the subscript m indicates the core to which the tensor will be referred. This expression can be written in terms of the expansion in TAOs

$$\begin{aligned} \langle \hat{J}_q^{(n)} \rangle_m &= \text{tr}[\sum_{\mu\nu} |\xi_\mu\rangle P_{\mu\nu} \langle \xi_\nu | (\hat{J}_q^{(n)})_m] \\ &= \sum_{\mu\nu} P_{\mu\nu} \langle \xi_\nu | (\hat{J}_q^{(n)})_m | \xi_\mu \rangle \end{aligned} \quad (5.7)$$

where we have employed the cyclic property of the trace. We further define the expectation value on core m by restricting the orbitals μ to be only those on core m. It can be shown, applying this formulation to the orientation parameters in the chosen geometry, that they are all identically equal to zero.

$$\begin{aligned}\langle \hat{j}_0^{(1)} \rangle_m &= \langle \hat{j}_z \rangle_m = 0 \\ \langle \hat{j}_{\pm 1}^{(1)} \rangle_m &= \langle \mp \frac{\hat{j}_{\pm 1}}{\sqrt{2}} \rangle_m = 0\end{aligned}\quad (5.8)$$

This would not necessarily be true if the collision geometry were such that the collision occurred in the x-y plane. Therefore, some of the workers in the field report orientations while, because of our choice of geometry, we will only report an alignment parameter. In our geometry the only alignment parameter with nonzero value is

$$\begin{aligned}A_0^{(2)}(J) &= \frac{\sqrt{6}}{J(J+1)} \text{Re} \langle \hat{j}_0^{(2)} \rangle_{m,t} \\ \hat{j}_0^{(2)} &= \frac{1}{\sqrt{6}} (3\hat{j}_z^2 - \hat{j}^2)\end{aligned}\quad (5.9)$$

We will be interested in reporting what is called the integral alignment, A_{20} for comparison to other theoretical and experimental results. The integral alignment is defined for a given projectile energy E

$$A_{20}(E) = \frac{\frac{1}{2}\sigma_x(E) - \sigma_z(E)}{\sigma_x(E) + \sigma_z(E)} \quad (5.10)$$

where $\sigma_x(E)$ and $\sigma_z(E)$ are the state-to-state integral cross sections at projectile energy E for the 2px and 2pz atomic orbitals at core m, respectively. The state-to-state integral cross section to a final atomic orbital μ for projectile energy E

is defined by

$$\sigma_\mu(E) = 2\pi \int_0^\infty b P_{\mu\alpha}(E, b) db \quad (5.11)$$

where b is the impact parameter and $P_{\mu\alpha}(E, b)$ is the transition probability from initial state α to final state μ at the final time.

Another concept from time-independent studies that will prove to be of interest for time-dependent studies is the idea of atomic population. It has been shown within a time-independent framework that the electronic population of an atomic state μ may be generally defined by [48]

$$N_\mu = \sum_{\nu\rho} (S^\alpha)_{\mu\nu} P_{\nu\rho} (S^{1-\alpha})_{\rho\mu} \quad (5.12)$$

where the choice of α is restricted to the interval $0 \leq \alpha \leq 1$. We will consider how these definitions perform as measures of time-dependent populations. The two particular choices of α with which we will concern ourselves define the so-called Mulliken and Löwdin population. The Mulliken population is defined by the choice of $\alpha = 0$ while the Löwdin population is defined by the choice of $\alpha = \frac{1}{2}$. The calculation of the Löwdin population involves finding the eigenvalues of the overlap matrix and hence requires a little more care in calculation than the Mulliken population; however, the calculation of populations requires very little of the actual computational time for any given collision so that time involved in population calculation will not be considered critical to the evaluation of differing population analyses.

The physical implications of the population analyses will be the principal criterion for this evaluation. It can be seen that we may now define the time-dependent alignment parameter in terms of the Mulliken population

$$A_0^{(2)}(t) = N_{2px}(t) - 2N_{2pz}(t) \quad (5.13)$$

This definition of alignment is seen to be an absolute rather than relative definition with regard to the total 2p population. In summary, these definitions of time-dependent properties have been chosen because of their close relationship to already familiar properties calculated in time-independent approaches. It is hoped that these time-dependent measures of atomic populations and electronic alignment will provide new insights into the most fundamental electronic rearrangement interactions.

CHAPTER 6

INTEGRATION OF THE LINEARIZED TDHF EQUATIONS

So far we have considered the derivation and development of a temporally linearized time-dependent Hartree-Fock description for the electronic density matrices in collision involving electronic rearrangement. In this chapter we will describe the calculational approach to the solution of the first-order differential equation in time previously derived for the motion of the cores, which are treated as classical particles within the eikonal approximation, and for the electronic densities, which are treated as quantum mechanical entities. It will be seen that the order in which the integrations are accomplished is essential to achieving the appropriate result. Further, the procedure for including the coupling between electronic and nuclear motions will be discussed in greater detail.

In chapter 4, we began the discussion of the criteria for the choice of an appropriate time step developed with particular consideration given to the electronic degrees of freedom. We recall that the time step Δt is chosen so that the condition

$$\epsilon_{lower} \leq \frac{||Q^\gamma||}{||P^\gamma||} \leq \epsilon_{higher} \quad (6.1)$$

is satisfied. The propagation of the core degrees of freedom require the solution of the Hamilton's equations, which need the knowledge of the core positions and

momenta at a given time and the potential in which the cores move. We have chosen to use the Runge-Kutta fourth order algorithm for the integration of these Hamilton's equations. It is important that the Runge-Kutta fourth order algorithm is self starting and can be adapted to use our choice of time step rather than needing a constant time step. This choice of integrator is by no means unique and perhaps may not be optimal, however for the purposes of our calculation the algorithm is known to be quite reliable. The integration of the core coordinates requires a small fraction of the total computing time involved in a typical computation so that we have not put a considerable amount of effort into the optimization of the core integrations.

Once we have chosen a test time step Δt , the time step is taken in two parts. First the time is advanced by one half of the total time step. As we know the full electronic density matrix at time t_0 , we may calculate the potential which depends on this density matrix at time t_0 . From the positions and momenta of the cores at time t_0 as well as the potential due to the electronic degrees of freedom, we are able to move the cores to their positions and momenta at time $t_{1/2} = t_0 + \frac{1}{2}\Delta t$. After the core coordinates have been calculated at time $t_{1/2}$, we are able to calculate the reference density at time $t_{1/2}$. With this new reference density, we are now ready to complete the time step. Completing the time step requires the calculation of the electronic potential at time $t_{1/2}$, which is done using the new reference density. Next the core coordinates are propagated to the end of

the time step t_1 . Having the core positions and momenta at time t_1 we are able to use the temporal linearization scheme to calculate the reference density and the change in the density at time t_1 . Schematically the procedure looks like this

$$\begin{aligned} \text{Given } (\mathbf{R}, \mathbf{P}, \rho, V)_{t_0} &\rightarrow \text{Advance to } t_{\frac{1}{2}} \rightarrow \\ \text{Calculate } (\mathbf{R}, \mathbf{P}, \rho^{(0)}, V)_{t_{\frac{1}{2}}} &\rightarrow \text{Advance to } t_1 \rightarrow \quad (6.2) \\ \text{Calculate } (\mathbf{R}, \mathbf{P}, \rho, V)_{t_1} \end{aligned}$$

If the condition on the change of the density matrix is not satisfied another time step is chosen. If the change of the density matrix is too small the original time step is tripled while if the change of the density matrix is too large the original time step is halved. Note that these choices of multiples for the time step avoid the possibility of 'trapping' in which the change in the density matrix is alternately too large then too small indefinitely. If the change in the density matrix is within tolerances the time step is accepted, time t_1 is then renamed time t_0 and the previous time step serves as a first guess to the next time step. When the separation between the cores exceeds an ending value the integration is completed and the final results of the computation are reported. The calculation of a single integrated cross section may require that the integration be carried out for as many as 100 impact parameters and that the transition probabilities be integrated over these impact parameters.

There is a considerable advantage to calculating each time step in two halves. The integral $\Gamma_{i\nu\rho j}$ which depends on the driving term in equation 4.15 can be

calculated to order Δt^2 by expanding the driving term around time $t_{1/2}$ rather than around time t_0 or time t_1 . In the calculations present here the driving term is expanded around time $t_{1/2}$ and terms of first order in time and of higher order are ignored leaving only the value of the driving term itself at time $t_{1/2}$. Tests have been carried out by keeping the first order term in time as well, but these tests showed no considerable difference in the calculation when run under the same initial conditions and given the same tolerances.

A series of test calculations have been run to ensure the convergence and stability of the numerical procedures for the integration of the equations for core and electronic density matrix propagation. These tests have involved varying of some parameters input to the calculation while holding others fixed. The parameters which have been tested include:

- the initial and final separation of the cores
- the higher and lower tolerances
- the initial time step
- the maximum time step

The choice of basis set for the calculation also plays an important role in the quality of the result. the next chapter will be dedicated to the discussion of the choice of basis set and the calculation of integrals in the various bases.

CHAPTER 7

CHOICE OF BASIS SET AND ITS EFFECT ON CALCULATION

The expansion of the density, overlap, and Fock operators into matrix form requires the choice of a set of basis functions in whose terms the atomic and molecular orbitals may be expanded. The choice of basis set has been dealt with extensively in the case of time-independent atomic and molecular structure calculations. A time-dependent dynamics calculation presents a series of problems that are not necessarily confronted in the time-independent case. The need for geometries far away from equilibrium as well as the large range of possible separations of the cores is one such problem. A second problem is the need for the inclusion of a large number of atomic and molecular states which are not in the ground state configuration. The need in time-dependent methods to calculate overlap and Fock matrix elements at the large number of differing geometries which occur over the course of the collision also separates dynamics and structural calculations. Finally, the need to interpret the final result in terms of the atomic orbitals of the products of the interaction puts a premium on an insightful choice of basis.

Recall equation 3.4, where we expanded the time-dependent molecular orbitals as linear combinations of traveling atomic orbitals

$$\phi_i^\gamma(\vec{r}_j, t) = \sum_{\mu} T_m(\vec{r}_j, t) \chi_\mu(\vec{r}_{mj}) c_{\mu i}^\gamma(t) \quad (7.1)$$

and used the local version of the electron translation factor

$$T_m(\vec{r}_j, t) = \exp[i m_e (\vec{v}_m \cdot \vec{r}_j - \frac{1}{2} \int_{t_0}^t v_m^2 dt')] \quad (7.2)$$

It is rather evident that as the core velocity \vec{v}_m tends to 0 the value of the ETF tends to 1. Hence it would be interesting to study the effect of the ETF in a few simple cases to determine at what core velocity it becomes appropriate to neglect ETFs. In Figures 7-1 and 7-2 we display the result of a calculation on the proton-Hydrogen atom system using the traveling atomic basis and the non-traveling, static atomic basis. Here we have used a basis which includes only the 1s hydrogenic orbital on each center and the screened Coulomb potential, as described in chapter 2, is used for the calculation of the nuclear trajectories.

The transfer probability is plotted versus the impact parameter at impact energies of 1 keV and 10 eV, respectively. It is clear that the result at 1 keV which corresponds to a velocity of 0.2 au is profoundly affected by the use of ETFs. The 10 eV result which corresponds to a velocity of 0.02 au shows less of a difference between TAO and AO bases as the two are distinguishable only at very small values of the impact parameter. We conclude therefore, that the

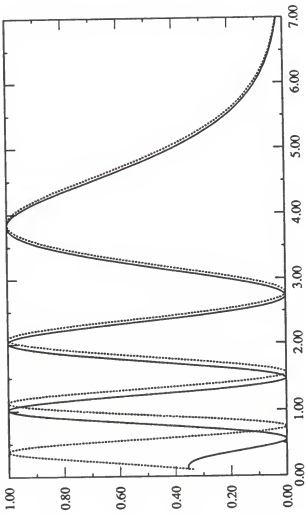


Figure 7-1: Transfer probability vs. Impact parameter in au for proton-Hydrogen atom collisions at a lab energy of 1 keV. (full line: including ETFs, dotted line: without ETFs)

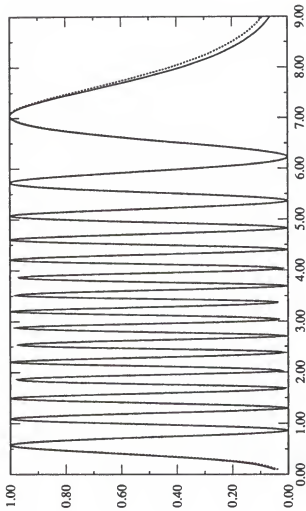


Figure 7-2: Transfer probability vs. Impact parameter in au for proton-Hydrogen atom collisions at a lab energy of 10 eV. (full line: including ETFs, dotted line: without ETFs)

use of ETFs for collision velocities of 0.02 au or below is not necessary in the calculation of integrals if one wishes to obtain correct integral cross sections. It is however necessary in the formalism to cancel spurious long-range couplings.

We have used two types of bases with and without ETFs for the representation of the electron density matrices in our time-dependent studies. The first is the exact hydrogenic basis in which we include the 1s, 2s, 2p_x, 2p_y, and 2p_z orbitals on each center. The overlap and Hamiltonian elements are programmed as a function of the effective charge of the core on which the orbital is centered. The integration of the overlap and Hamiltonian matrix elements involving two centers was carried out over elliptical coordinates defined by

$$\begin{aligned}\xi &= \frac{1}{R}(r_{aj} + r_{bj}) \\ \eta &= \frac{1}{R}(r_{aj} - r_{bj}) \\ \varphi &= \varphi_a = \varphi_b \\ dv &= \frac{R^3}{8}(\xi^2 - \eta^2)d\xi d\eta d\varphi\end{aligned}\tag{7.3}$$

where the ranges of integration are

$$1 \leq \xi < \infty ; -1 \leq \eta \leq 1 ; 0 \leq \varphi \leq 2\pi\tag{7.4}$$

Here we have defined the separation between centers a and b to be R, the electron coordinate referred to center a to be r_{aj} , and the electron coordinate referred to center b to be r_{bj} . The azimuthal angle is taken to be φ and the coordinate system is oriented so that the z-axis is along the intercenter axis and the x-axis is in the

plane of the collision. The resulting integrals in this coordinate system need to be rotated to the frame in which the time propagation is being performed. This is accomplished by a rotational similarity transformation among integrals involving p-type orbitals as given in Goldstein's *Classical Mechanics*, chapter 6 [49]. The rotation is performed around the y-axis through the angle between the intercenter axis and the time propagation's z-axis. The result of the integrations of hydrogenic orbitals for overlap and Hamiltonian matrix elements is presented in Appendix A as a function of intercenter separation and effective core charge.

A popular choice of basis set for time-independent calculations is the basis of Gaussian type orbitals. It has been shown by Boys [50] that the use of Gaussian type orbitals allows for the rapid calculation of one- and two-electron integrals in the context of time-independent Hartree-Fock theory. It seems natural to employ a similar strategy in time-dependent calculations. This strategy entails writing of atomic orbitals in the form (after scaling to eliminate charge parameters) [51]

$$\phi_{nl\eta}(1, \vec{r}_{mj}) = \sum_k^K d_{nl,k} g_{nl\eta}(\alpha_{nl,k}, \vec{r}_{mj}) \quad (7.5)$$

where $\eta = x, y, z$. Here the Gaussian-type orbital for g_{1s} , g_{2p_x} , g_{2p_y} and g_{2p_z} are

$$\begin{aligned} g_{1s}(\alpha, \vec{r}_{mj}) &= \left(\frac{2\alpha}{\pi}\right)^{\frac{3}{4}} \exp(-\alpha r_{mj}^2) \\ g_{2p_x}(\alpha, \vec{r}_{mj}) &= \left(\frac{128\alpha^5}{\pi^3}\right)^{\frac{1}{4}} x_{mj} \exp(-\alpha r_{mj}^2) \\ g_{2p_y}(\alpha, \vec{r}_{mj}) &= \left(\frac{128\alpha^5}{\pi^3}\right)^{\frac{1}{4}} y_{mj} \exp(-\alpha r_{mj}^2) \\ g_{2p_z}(\alpha, \vec{r}_{mj}) &= \left(\frac{128\alpha^5}{\pi^3}\right)^{\frac{1}{4}} z_{mj} \exp(-\alpha r_{mj}^2) \end{aligned} \quad (7.6)$$

where the number K ranges in our studies from 3 to 6, $\alpha_{nl,k}$ are the Gaussian exponential coefficients, and $d_{nl,k}$ are the expansion coefficients. The Slater-type orbitals are identical to hydrogenic orbitals for the 1s and 2p orbitals. For the 2s orbital the use of Slater-type orbitals written as linear combinations of Gaussian-type orbitals is not sufficient as the 2s Slater-type orbital is nodeless. Therefore, Gaussian exponential coefficients and expansion coefficients have been chosen to fit the hydrogenic 2s function rather than the Slater-type function.

There are a number of available integral packages for the integration of Gaussian-type orbitals. We have chosen to use the MOLECULE package developed by Jan Almlöf and P. R. Taylor [52]. The local VMOL package calculates both one- and two-electron integrals for either segmented contracted or generally contracted orbitals. We have chosen to use segmented contracted sets of Gaussians to represent the 1s, 2s and 2p hydrogenic orbitals for a given effective charge.

The VMOL package writes the results for a given geometry to integral files. This would necessitate numerous input/output operations in our time-dependent code which could be quite time consuming. Hence, we have modified the MOLECULE package to write the results of integral calculations into the appropriate arrays and made the subroutine calls internal to our main program so that we are able to calculate the integrals at the large number of geometries we require and save the computing time that would otherwise be devoted to MOLECULE input/output.

We have also tested the effect of varying the number of Gaussians used to approximate the hydrogenic orbitals. In Figure 7-3 we show the transfer probability versus impact parameter for a proton colliding with a hydrogen atom in its ground state.

This calculation was carried out at an impact energy of 1 keV using from 3 to 6 Gaussians to represent the 1s orbital of hydrogen. Only the 1s orbitals on each center were used for this calculation. Also included is the result using the exact 1s hydrogenic on each center. We see that the agreement in general is rather good while there is a distinct improvement in moving from 3 to 4 Gaussians per orbital the improvement beyond 4 is only marginal and integrated cross sections would not be markedly improved. We move now to the consideration of inclusion of electron translation factors in the one-electron integrals.

The inclusion of ETFs in two-center, one-electron integrals done over hydrogenic orbitals is problematic because the integrations cannot be carried out analytically. Various numerical procedures have been implemented which require the numerical integration over one or two variables. Another option that has been tried in the literature is to write the orbitals as linear combinations of Gaussians. In this scheme the analytical forms of the integrals can be obtained and the approximation occurs only in the fitting of the Gaussians to the actual orbitals of interest. We have expanded the work of McWeeny by including higher angular momentum states and adding a version of the 2s orbital similar in form to the 1s

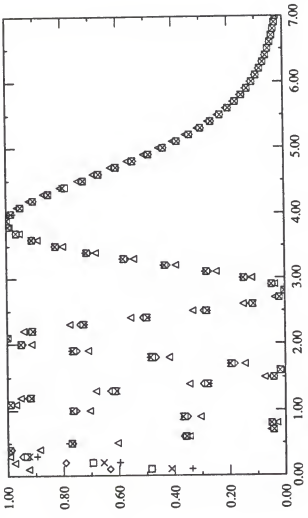


Figure 7-3: Electron transfer probability vs. Impact parameter in au (plus: exact 1s hydrogenic; triangle: 3 Gaussians; diamond: 4 Gaussians; box: 5 Gaussians; cross: 6 Gaussians)

orbital rather than McWeeny's choice of 2s orbital which is of the form [53]

$$g_s(\alpha, \vec{r}_{mj}) = \left(\frac{2\alpha}{\pi}\right)^{\frac{3}{4}} r_{mj}^2 \exp(-\alpha r_{mj}^2) \quad (7.7)$$

The derivation of the higher angular momentum states is greatly aided by the observation that the Gaussian basis functions of one angular momentum are related to the derivative of those of lower angular momentum states. Given that

$$g_s(\alpha, \vec{r}_{mj}) = \left(\frac{2\alpha}{\pi}\right)^{\frac{3}{4}} \exp(-\alpha r_{mj}^2) \quad (7.8)$$

if we take the derivative of the s-state Gaussian with respect to a coordinate of the center m we obtain

$$\begin{aligned} \frac{d}{d\eta_m} g_s(\alpha, \vec{r}_{mj}) &= \left(\frac{2\alpha}{\pi}\right)^{\frac{3}{4}} \alpha \eta_m \exp(-\alpha r_{mj}^2) \\ &= \sqrt{\alpha} g_{p_\eta}(\alpha, \vec{r}_{mj}) \end{aligned} \quad (7.9)$$

where the index η runs over the x, y, and z coordinates of center m. Similarly, we have that taking the derivative of the p-type Gaussian with respect to the coordinates of the center m

$$\frac{d}{d\zeta_m} g_{p_\eta}(\alpha, \vec{r}_{mj}) = \sqrt{\alpha} g_{d_{\eta\zeta}}(\alpha, \vec{r}_{mj}) \quad (7.10)$$

It should be mentioned at this point that our time-dependent program was altered to accommodate complex orbitals so that the ETFs could be incorporated. There is now an obvious scheme for the calculation of the two-center overlap integrals in which they are related to s-type overlaps with differing Gaussian exponential

coefficients and coefficients derived by differentiation. The results of these operations appear in Appendix B.

We now need to turn our attention to the problem of calculating two-center Hamiltonian matrix elements including ETFs. The most important difficulty, that of calculating the core-electron interaction, has been addressed by other authors. Their approaches rely on a number of approximations that we either are unable to make or would prefer not to make. We will avoid the problem of the calculation of the core-electron interaction by making the following observation. We write the Hamiltonian operator in the following suggestive form

$$\hat{H} = \hat{T} + \hat{V}_m + \hat{T} + \hat{V}_n - \hat{T} \quad (7.11)$$

where we have added and subtracted the kinetic energy operator \hat{T} . Taking the matrix element of \hat{H} between traveling atomic orbitals on two differing centers we obtain

$$H_{\mu\nu} = (\epsilon_\mu + \epsilon_\nu) S_{\mu\nu} - \langle \xi_\mu | \hat{T} | \xi_\nu \rangle \quad (7.12)$$

where ϵ_μ is the eigenenergy of the orbital ξ_μ for its appropriate asymptotic Hamiltonian

$$\begin{aligned} \hat{H}_m &= \hat{T} + \hat{V}_m \\ \hat{H}_m \xi_\mu &= \epsilon_\mu \xi_\mu \end{aligned} \quad (7.13)$$

The problem of calculating two-center, one-electron Hamiltonian elements now reduces to the more tractable problem of calculating the kinetic energy matrix

elements which may in turn be related to the two-center, one-electron overlap integral previously discussed. The results of these derivations are also presented in Appendix B.

Testing of the two-center overlap and one-electron Hamiltonian elements has included the comparison of traveling atomic orbital calculation to static atomic orbital calculation in the zero velocity limit. Agreement to at least 9 decimal places was found between our calculations and calculations made for the same Gaussian basis using the MOLECULE program package. Further testing involved the calculation of overlap and Hamiltonian matrix elements for a small basis and checking these results by hand. These results agreed to at least 7 decimal places, where the hand calculations were restricted by the accuracy of the calculator used.

CHAPTER 8

APPLICATIONS I: THE PROTON-HYDROGEN ATOM SYSTEM

Overview of Experimental Methods

We first applied our method to the simplest of collisional systems consisting of two protons and one electron, that is the collision of an incident proton on a target Hydrogen atom. Despite its apparent simplicity, this system has not been solved exactly and hence, has inspired a great deal of theoretical and experimental study. Properties of interest for these collisions are the total integral cross section, the state-to-state integral cross section, and the differential cross section for electron transfer, electron transfer excitation, and direct electron excitation. Integral alignment, as described in chapter 5, has also been of theoretical and experimental interest. Energies of interest for the incident proton have ranged from as low as 1 eV to greater than 1 MeV. We concern ourselves with the lower end of this range, that is 2 keV and below. We will discuss the role of electron translation factors, basis set type and size, and choice of electronic potential in regard to their effect on the calculation of the above quantities of interest. We will also discuss the relative difficulties of correct calculation of these quantities over the entire energy range of interest.

The numerous experiments that have been carried out on this system can be divided into five categories which depend on the way the protons interact with the Hydrogen atoms and the way the final states are detected. There are two experimental geometries for the interaction

- The high energy proton beam is incident on a thermal energy target Hydrogen atom beam, a crossed beam geometry.
- The proton beam and the target Hydrogen atom beam travel through an interaction region together, a merging beam geometry.

Detection apparatus vary according to the quantity to be measured. There are four detector arrays considered here

- An ion or atom counting mechanism collects the forward scattered projectiles and sorts them according to their charge, a counter.
- A polarization sensitive photon counter collects radiation given off by either projectile or target atoms, a Lyman- α detector.
- A quenching electric field is applied to the collision region and radiation collected, a quenched Lyman- α detector.
- An ion counter and an atom counter are used to analyze projectile beams selected by their scattering angle, a differential detector.

The combination of a crossed beam geometry and a counter detector allows the measurement of total integral cross sections at fairly high energies [54–57].

The combination of a crossed beam geometry and a Lyman- α detector allows the measurement of state-to-state integral cross section to 2p states and integral alignments [58, 46, 59, 60]. The combination of a crossed beam geometry and a quenched Lyman- α detector allows the measurement of state-to-state integral cross sections to 2p and 2s states [61–64]. The combination of a crossed beam geometry and a differential detector allows the measurement of differential cross sections [65]. Finally, the combination of a merging beam geometry and a counter detector allows the measurement of total integral cross sections at lower energies [66].

Integral Cross Sections

The determination of total integral cross section at higher energies is a deceptively easily calculated quantity. A comparison of theoretical and experimental values obtained in the case of a 1 or 2 keV projectile incident on Hydrogen atom is shown in table 8–1. Table 8–1 illustrates that the total integral cross section at an intermediate energy is quite easily calculated to an accuracy of 20% or less. This raises the question of why this should be true even for theoretical methods which use only the 1s orbital on each center. A more detailed study of the role of basis set size and type and the role of the potential in which the nuclei move may enhance our insight as to why this should be. Figure 8–1 shows the influence of

the choice of nuclear trajectory on a calculation at 1 keV with a 1s hydrogenic orbital per center .

It is obvious that the choice of nuclear trajectory does not impact the calculational result in the case of the 1 keV collision. The question becomes: is the choice of nuclear trajectory ever important for the calculation of total integral cross sections? It becomes apparent that the choice of nuclear trajectory is likely to be more important as the projectile energy is lowered. The effect of the screened Coulomb potential is expected to allow for some curvature in the trajectory but not as much curvature as would be expected from the Coulomb potential. We therefore present in Figure 8-2 a comparison of nuclear trajectories at an impact energy of 100 eV. Again, the calculation includes a 1s hydrogenic orbital per center.

Here we see that at the lower energy of 100 eV the zero potential is closer to the screened Coulomb potential than the Coulomb potential. It is anticipated that the screened Coulomb potential will do the best job in calculating total integral cross sections at lower energies. We will come back to this assertion in good order. We now continue to examine the role of the choice of nuclear trajectory at lower energies by comparing these choices at 10 eV. In Figure 8-3 we show a comparison of the results for these trajectory choices at an impact energy of 10 eV.

Here we see that the three trajectory choices give very different results with the Coulomb potential departing most from the screened Coulomb potential. A

Table 8.1: A comparison of experiment and theory for total integral cross sections.

Total Integral Cross Section $\times 10^{16}$ cm 2 Theory and Experiment			
	Experiment	1 keV	2 keV
[57]		16.3 \pm 18%	13.9 \pm 17%
[54]		19.0 \pm 20%	18.0 \pm 20%
[56]		20.2 \pm 20%	13.5 \pm 20%
Theory			
Present work		17.0	14.7
[1]		16.5	N/A
[8]		16.3	N/A
[21]		19.1	14.8
[9]		16.9	14.2
[5]		N/A	14.5 \pm 0.5
[22]		14.9	12.6
[39]		16.78	14.07

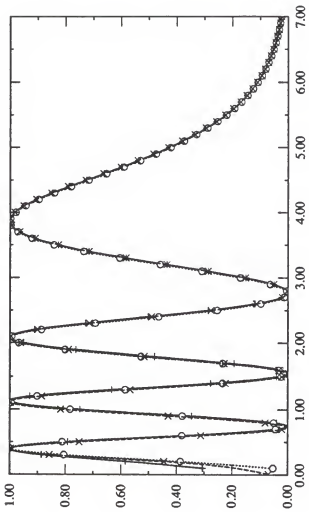


Figure 8-1: Transfer probability vs Impact parameter in au for a 1 keV proton-Hydrogen atom collision (plus: zero potential; circle: Coulomb potential; cross: screened Coulomb potential)

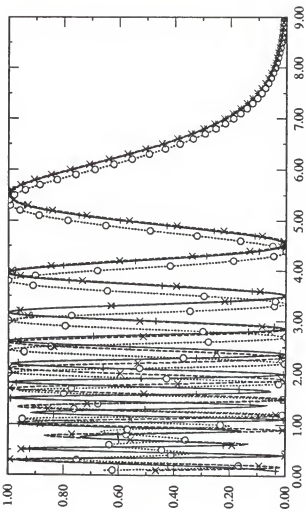


Figure 8-2: Transfer probability vs Impact parameter in au for a 100 eV proton-Hydrogen atom collision (plus: zero potential; circle: Coulomb potential; cross: screened Coulomb potential)

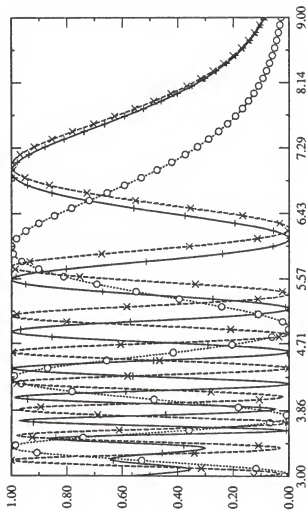
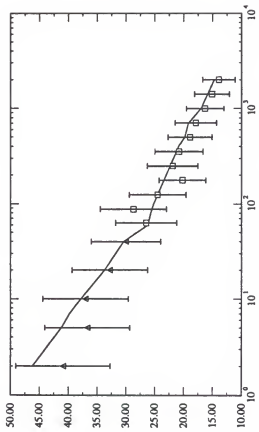


Figure 8-3: Transfer probability vs Impact parameter in au for a 10 eV proton-Hydrogen atom collision (plus: zero potential; circle: Coulomb potential; cross: screened Coulomb potential)

stricter test of the quality of the trajectory is the comparison with differential cross sections measured by experiment which we will deal with later in this chapter. Now let us complete our discussion of total integral cross section, in Figure 8-4 we show a comparison of total integral cross section between our results and experiments.

Note that the agreement between calculated and experimental results is good through the entire range of projectile energies from 2 to 2000 eV. This is another bit of evidence that the screened Coulomb potential is the best choice for this system as a poorer choice of potential would not give good agreement over so wide a range of energies, particularly at lower energies.

We now move on to state-to-state integral cross sections. The role of electron translation factors in these calculations, which was discussed in chapter 7, is also important in obtaining accurate values for state-to-state integral cross sections. ETFs are most important in the calculation of integral alignments which will be discussed below. Table 8-2 shows a detailed comparison of various experimental and theoretical results in a 2 keV impact of a proton on a target Hydrogen atom. This comparison shows that our theoretical results are in good agreement with experiment for all state-to-state integral cross sections. Note that the predominate mechanism for charge transfer is the resonant transfer channel, this helps to explain why total electron transfer integral cross sections are so easily found to within 20% theoretically. The most difficult state-to-state cross sections to obtain accurately



References: squares: [57], triangles: [66]

Figure 8-4: Total integral cross section vs Projectile energy (eV)
comparison between our theoretical results and those of experiment

Table 8.2: Comparison of theoretical and experimental results for state-to-state integral cross sections for a 2 keV proton incident on a Hydrogen atom.

$H^+ + H$ State-to-state Integral Cross Sections (10^{-16} cm^2) at E=2 keV (SCP)						
Target	Present Work	R & D [9]	L & D [22]	F & L [14]	D. et al. [39]	Exps.
2s	0.0799	0.059	0.012	0.0224	0.06	0.10 ± 0.02 [63], 0.05 ± 0.02 [61]
2px	0.2890	0.280	0.265	0.264	NA	NA
2pz	0.0367	0.031	0.011	0.008	NA	NA
2p	0.3257	0.311	0.266	0.272	0.34	0.29 ± 0.07 [58]
Projectile						
1s	13.5495	13.92	12.3	NA	14.07	NA
2s	0.0112	0.057	0.013	0.021	0.01	NA
2px	0.3313	0.283	0.275	0.275	NA	NA
2pz	0.0625	0.030	0.011	0.008	NA	NA
2p	0.3938	0.313	0.286	0.287	0.29	0.33 ± 0.07 [58]
TOTAL	13.9545	14.389	12.599	NA	14.37	$13.9 \pm 17\%$ [57]

Table 8.3: Comparison of theoretical and experimental results for integral alignments in proton-Hydrogen atom collisions

$H^+ + H$ Integral Alignments (%) (SCP)						
Energy	Present Work	R & D [9]	L & D [22]	F & L [14]	D <i>et al.</i> [39]	Exps.
2 keV	33.1	35.0	43.8	45.5	33	39 ± 10 [46], 10 ± 20 [59]
1 keV	40.0	40.4	46.8	NA	30	32 ± 10 [46]
700 eV	12.3	32.7	NA	NA	NA	NA
500 eV	4.8	34.8	NA	NA	23	NA

are the $2s$, $2p_x$, and $2p_z$ which require the inclusion of ETFs in our method. Note that all other theoretical methods in this comparison include ETFs in one way or another. Another experimentally measurable quantity that allows us to test the sensitivity of our results is the integral alignment. Accurate calculation of integral alignments requires a basis set which includes ETFs and has sufficient size to give a good description of the $n=2$ orbitals of the Hydrogen atom. In this study of integral alignment our basis set has consisted of 5 hydrogenic orbitals per center each written as a sum of 6 Gaussian orbitals. The 5 hydrogenic orbitals that were used include the $1s$, $2s$, $2p_x$, $2p_y$, and $2p_z$. Table 8-3 shows a comparison of theoretical and experimental results for integral alignments for a number of energies in the proton-Hydrogen atom system.

Here the result of Fite *et al.* [59] appears to be anomalous. Our result agrees well with Hippler's [46] at both available energies. We also predict a drop in integral alignments at lower energies, a prediction made by Deumens *et al.* [39] as well, however the exact energy at which the drop in integral alignment occurs is not agreed upon, Deumens *et al.* [39] see a drop below 500 eV. It is appropriate to keep in mind that at lower energies the excitation cross section amount to less than 0.1% of the resonant transfer cross section so that the integral alignments at these lower energies will be very difficult to measure experimentally.

Differential Cross Sections

The final experimental verification of the soundness of our theoretical method comes from the examination of differential cross sections. A comparison of the effect of choice of potential on differential cross section is shown in Figures 8-5 and 8-6. We introduce the reduced differential cross section ρ as defined by Houver *et al.* [65]

$$\rho = \sigma \theta_L \sin \theta_L \quad (8.1)$$

where σ is the differential cross section in au and θ_L is the lab scattering angle in degrees. Figure 8-5 shows the elastic reduced differential cross section versus lab angle in degrees for the screened Coulomb potential, the Coulomb potential and the the experimental result of Houver *et al.* [65] at a projectile energy of 410 eV. Figure 8-6 shows the charge transfer reduced differential cross section versus lab angle in degrees.

It is necessary to note that the experiment by Houver *et al.* [65] has an angular resolution of 0.2 degrees at small angles but at larger angles the resolution drops to 1.2 degrees. Hence it is quite likely that the calculated minimum in the elastic reduced differential cross section at about 4 degrees would be missed by the experiment. There is substantial agreement between our work and the experiment in term of the maxima around 1.5 degrees and 3.0 degrees and the large angle trend around 7 degrees seems to show good agreement. The calculation of differential

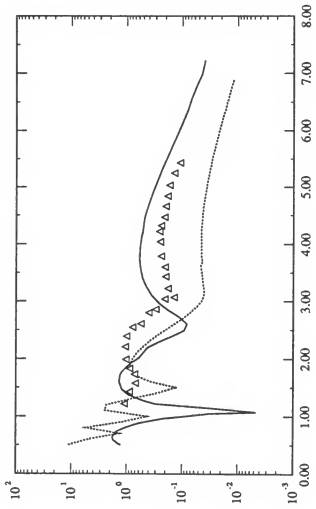


Figure 8-5: Elastic reduced differential cross section vs lab angle for a 410 eV proton incident on a Hydrogen atom target (full line: SCP; dotted line: CP; triangles: [65])

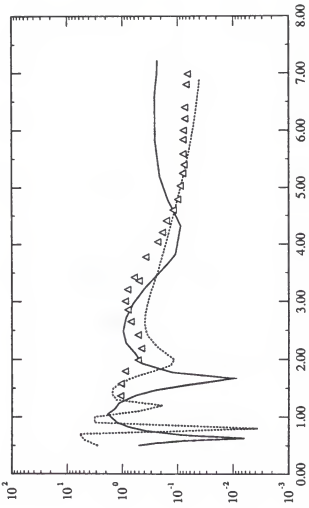


Figure 8-6: Charge transfer reduced differential cross section vs lab angle for a 410 eV proton incident on a Hydrogen atom target [full line: SCP; dotted line: CP; triangles: [65]]

cross section vs. scattering angle is quite sensitive to the choice of effective potential. Choosing the Coulomb potential leads to scattering angles which are about twice as large as those calculated using the screened Coulomb potential. Obviously, the use of the zero potential is meaningless as it leads asymptotically to a zero scattering angle for any impact parameter. We conclude, therefore that the choice of the screened Coulomb potential is essential for accurate calculation of differential cross section at all energies of interest. We continue to compare our results using the screened Coulomb potential with those of experiment. It should be noted that Houver used a "best fit" to other theoretical results. It is not surprising that our results show a consistent 0.4 degree difference in the positions of extrema with their results. The most important features for comparison are the general features of the reduced differentail cross sections and the difference in angle between maxima and minima. Figures 8-7 and 8-8 present a comparison of our calculated results using the screened Coulomb potential and those of experiment for elastic and charge transfer reduced differential cross sections versus lab angle in degrees for 500 eV and 700 eV projectiles, respectively.

Again we note the agreement with the experimental results with respect to the type and spacing of the extrema of the reduced differential cross sections.

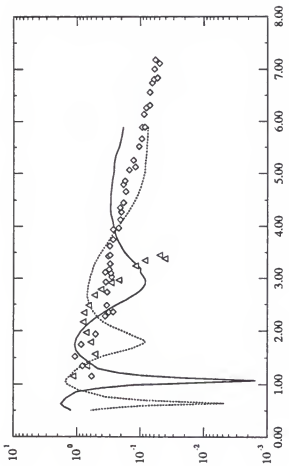


Figure 8-7: Elastic and charge transfer reduced differential cross section vs lab angle for a 500 eV proton incident on a Hydrogen atom target [full line: elastic; dotted line: charge transfer; triangles: experimental elastic; diamonds: experimental charge transfer; experimental results from [65]]

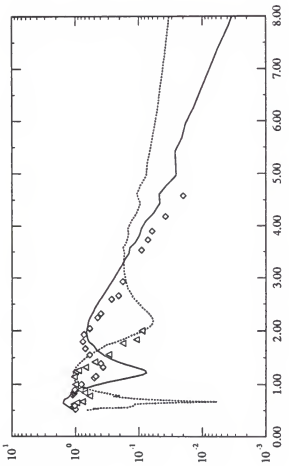


Figure 8–8: Elastic and charge transfer reduced differential cross section vs lab angle for a 700 eV proton incident on a Hydrogen atom target [full line: elastic; dotted line: charge transfer; triangles: experimental elastic; diamonds: experimental charge transfer, experimental results from [65]]

We now move on to consider the time dependent measures of atomic population discussed in chapter 6. We begin with a comparison of Mulliken and Löwdin populations. Figures 8–9 and 8–10 present a comparison of the time evolution of the Mulliken and Löwdin population in a 1 keV proton-Hydrogen atom collision, respectively. The impact parameter is 0.2 au, the zero of time is chosen to occur at the distance of closest approach, and the screened Coulomb potential has been used.

Note that the Mulliken population is occasionally greater than 1 or less than 0. This is not a behavior we desire in our measure of atomic population. As the Löwdin population does not show these pathologies we will prefer the Löwdin population as a measure of atomic population as a function of time. Figures 8–11 through 8–17 show the time evolution of the Löwdin populations of the other target and projectile states involved in this calculation. Note that the 2p_y orbital is not shown as it is never populated by the chosen geometry of the calculation.

Notice that all the populations oscillate before finally coming to a final asymptotic value which depends, of course, on the energy of the collision and the impact parameter. This is an example of the type of physical insight that we wish to obtain from time-dependent studies. This insight is again illustrated in Figures 8–18 and 8–19 in which the target 1s population's time evolution is

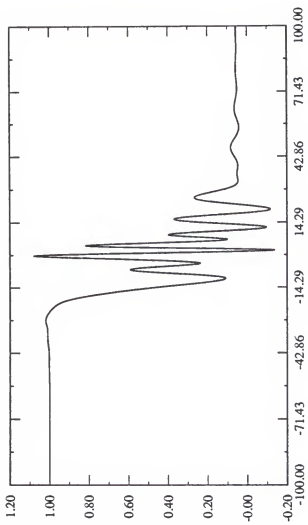


Figure 8-9: Mulliken population of the target 1s state vs time in au in a 1 keV proton-Hydrogen atom collision, at $b=0.2$ au

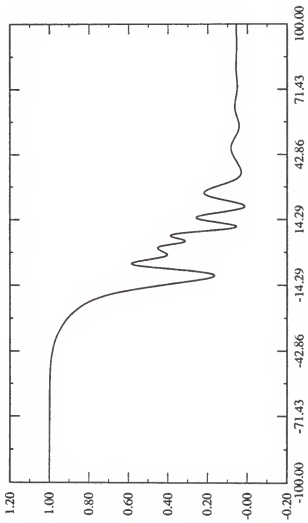


Figure 8–10: Löwdin population of the target 1s state vs time in au in a 1 keV proton-Hydrogen atom collision, at $b=0.2$ au

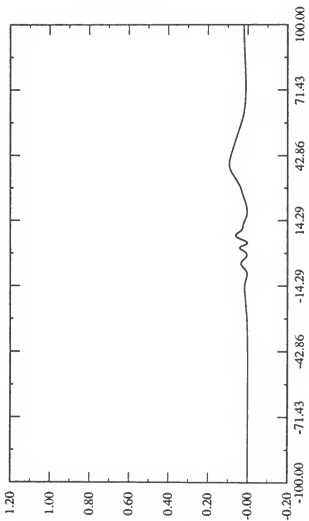


Figure 8-11: Löwdin population of the target 2s state vs time in au in a 1 keV proton-Hydrogen atom collision, at $b=0.2$ au

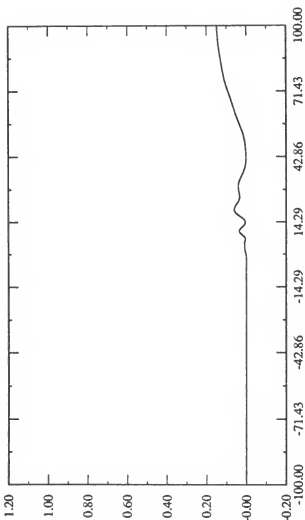


Figure 8-12: Löwdin population of the target $2p_x$ state vs time in au in a 1 keV proton-Hydrogen atom collision, at $b=0.2$ au

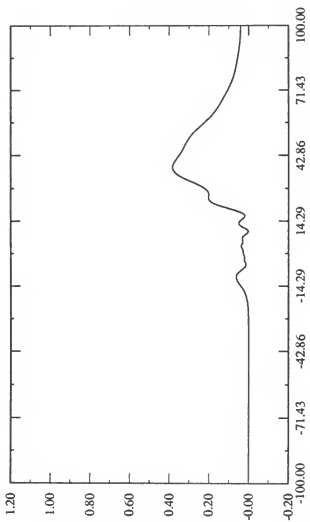


Figure 8-13: Löwdin population of the target $2p_z$ state vs time in au in a 1 keV proton-Hydrogen atom collision, at $b=0.2$ au

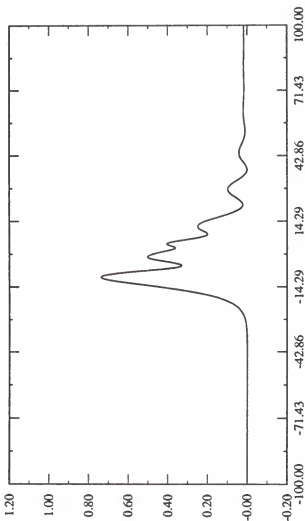


Figure 8–14: Löwdin population of the projectile 1s state vs time
in au in a 1 keV proton-Hydrogen atom collision, at $b=0.2$ au

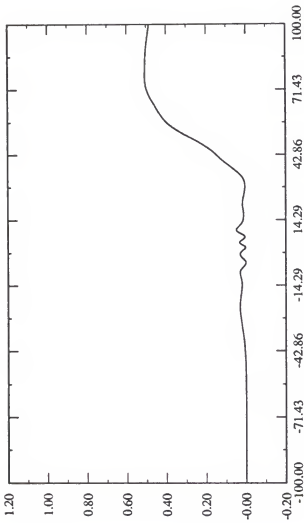


Figure 8-15: Löwdin population of the projectile 2s state vs time in au in a 1 keV proton-Hydrogen atom collision, at $b=0.2$ au

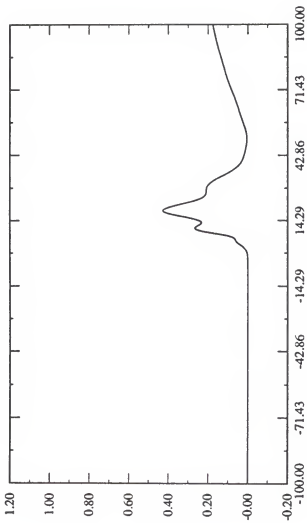


Figure 8–16: Löwdin population of the projectile $2p_x$ state vs time in au in a 1 keV proton-Hydrogen atom collision, at $b=0.2$ au

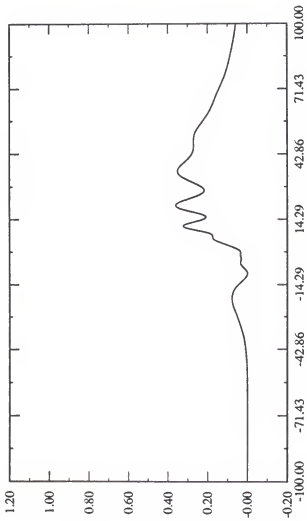


Figure 8-17: Löwdin population of the projectile $2p_z$ state vs time in au in a 1 keV proton-Hydrogen atom collision, at $b=0.2$ au

shown for a 10 eV proton-Hydrogen atom collision for impact parameters of 1.0 au and 1.2 au, respectively.

Here we see multiple oscillations in the target atom population as a function of time. We also notice that a slight change in the impact parameter causes a large change in the result of the collision, in this case a change of 0.2 au in the impact parameter makes the difference between complete retention of the electron by the target and complete transfer to the projectile. Because of the low collision energy there is no direct or transfer excitation.

The final time-dependent quantity that we investigate is the alignment parameter derived in chapter 6. To study the time evolution of the alignment of the target we need to consider a fairly high collision energy. In Figure 8-20 we present the time evolution of the alignment in a 1 keV collision at an impact parameter of 0.2 au.

Here we see that the alignment parameter also oscillates during the collision and is actually quite negative in the midst of the collision despite the fact that the alignment parameter for this collision is positive.

In summary, we have seen in this chapter that the total integral cross section at fairly high energies is the least demanding quantity to be accurately calculated. The differential cross section requires a realistic choice of electronic potential for accurate determination. The state-to-state integral cross section requires a traveling atomic basis for accurate calculation. Finally, we have seen that

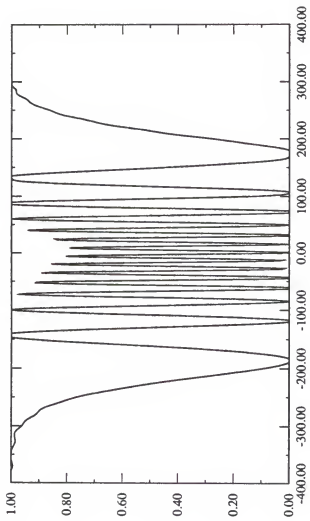


Figure 8–18: Löwdin population of the target 1s state vs time in au in a 10 eV proton-Hydrogen atom collision, at $b=1.0$ au

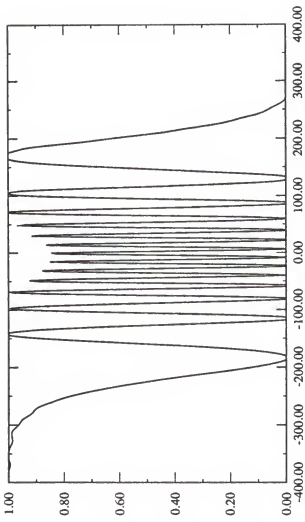


Figure 8-19: Löwdin population of the target 1s state vs time in au in a 10 eV proton-Hydrogen atom collision, at $b=1.2$ au

physical insight can be gained by examining atomic populations, where the Löwdin population is preferred over the Mulliken population, and by examining the alignment parameter vs. time.

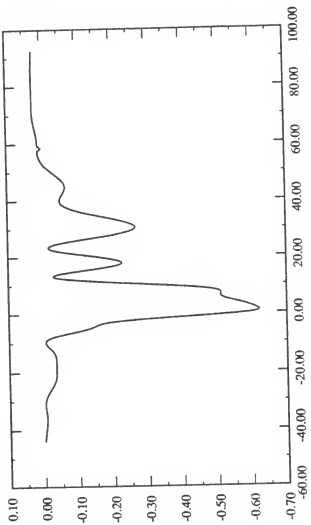


Figure 8–20: Alignment parameter vs time in au in a 1 keV proton-Hydrogen atom collision, at $b=0.2$ au

CHAPTER 9

APPLICATIONS II: THE HELIUM(2+)-HYDROGEN ATOM SYSTEM

A second system of interest for us is the collision of a fully stripped helium ion with a target Hydrogen atom. This system is an example of near resonant collisions in which the electron transfer is predominately from the H 1s state to the He^+ 2s or 2p state which are of equivalent asymptotic energy as the original system. As the nuclei are not of the same type the collision is not truly resonant as is the case considered in chapter 8. We will examine the projectile energy range from 1 keV to 8 keV. Again the integral charge transfer cross section and state-to-state integral cross sections will be of interest as well as time-dependent properties.

Experiments on this system can be described in terms of the categories introduced in chapter 8. The combination of crossed beam geometry and counter detection allows the measurement of total charge transfer integral cross section [67]. The combination of crossed beam geometry and counter and Lyman- α detection allows the measurement of total charge transfer integral cross section, direct measurement of 2p integral cross section and indirect measurement of 2s integral cross section [68–70]. The combination of crossed beam geometry and counter, Lyman- α and quenched Lyman- α detection allows the measurement of

total charge transfer integral cross section and direct measurement of 2p and 2s integral cross sections [71].

We have used a basis which includes the 1s, 2s, 2p_x and 2p_z hydrogenic orbitals on both the projectile and target nuclei. All calculations have been made using the zero potential, as the energy range is high enough that the calculation with the average effective potential would not improve the final integral cross sections significantly. ETFs have been included by writing the hydrogenic orbitals as linear combinations of 6 Gaussian orbitals each. We have investigated the projectile energies of 1 keV, 3 keV, and 8 keV. Table 9-1 presents a comparison of our results with various experimental and theoretical results at these energies.

The agreement with experiment is quite good although our results are consistently lower than some of the other accurate theories. The lack of the inclusion of the n=3 shell orbitals in our calculations may help explain this discrepancy. The results due to Rapp [10] are rather puzzling as he uses hydrogenic orbitals which include ETFs and his approach gave good agreement with ours in the proton-Hydrogen atom system. The calculation of state-to-state integral cross sections is a more demanding exercise. Table 9-2 presents a comparison of theory and experiment for state-to-state integral cross sections at a projectile energy of 8 keV.

The agreement between our state-to-state integral cross section results is again much better than those of Rapp [10]. The slight difference between our results and other accurate theories may also be a result of the differing basis sizes, as

Table 9.1: A comparison of experiment and theory of charge transfer integral cross section

He ²⁺ + H Integral Transfer Cross Section (10 ⁻¹⁶ cm ²) (ZP)							
Energy	Theory				Experiment		
	Present Work	H et al. [18]	K & T [20]	L & D [23]	R [10] [71]	S & G [67]	N et al. [68]
8 keV	5.19	6.30	6.15	6.26	NA	6.0 ± 1.0	5.0 ± 0.5 0.45
3 keV	0.606	1.49	1.43	NA	3.42	NA	0.84 ± 0.10
1 keV	0.0504	0.265	0.260	NA	1.40	NA	NA

Table 9.2: Comparison of theoretical and experimental results for state-to-state integral cross section for an 8 keV He^{2+} projectile incident on a Hydrogen atom.

State-to-state integral cross sections at 8 keV in $\text{He}^{2+}\text{-H}$ (10^{-16} cm^2)						
	Theory				Experiment	
	Present Work	H et al. [18]	K & T [20]	L & D [23]	R [10]	S & G [71] B & K [70]
2s	1.71	1.27	1.21	1.76	2.3	0.96 ± 0.2 $0.6 \pm 40\%$
2p	3.48	4.69	4.67	4.50	8.2	5.0 ± 1.0 $3.7 \pm 30\%$

above. We see that the agreement between theoretical results and experiment are really quite good. Comparison of state-to-state integral cross section at the lower energies is not presented due to a lack of experimental data.

Time-dependent phenomena that are of interest for this system include the alignment of the projectile and the electronic population of the target 1s state and the projectile 2s, 2p_x and 2p_z states. Figures 9-1 through 9-4 show the Löwdin populations of the target and projectile states. The conditions in this calculation have been chosen to correspond to the results shown in the previous chapter for the proton-Hydrogen atom system. This system, therefore, is the collision of a 4 keV He²⁺ with a target hydrogen at an impact parameter of 0.2 au. Notice that at this energy and impact parameter the charge exchange occurs primarily to the 2p_z state. By comparison to the previous chapter's results we see that there is less oscillation of the electronic population in the current near resonant collision than there was in the previous resonant case. However, there still is significant oscillation particularly in the 1s target and 2p_z projectile states. The variation in time of the alignment parameter is shown in Figure 9-5. This parameter shows pronounced oscillations much like those shown in the previous chapter. In this case, the alignment parameter is more negative than in the proton-Hydrogen atom collision. Again, we gain considerable insight into the charge transfer mechanism as a function of time in the collision of an ion with an atom.

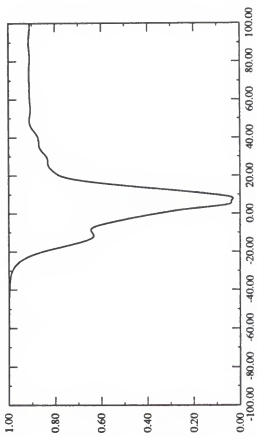


Figure 9-1: Löwdin population of the target 1s state vs time in au in a 4 keV He^{2+} -Hydrogen atom collision at $b=0.2$ au

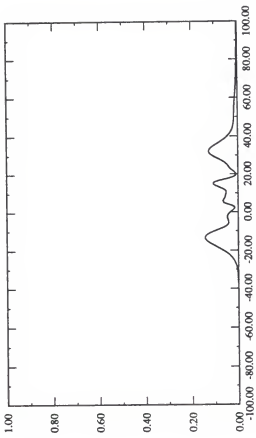


Figure 9-2: Löwdin population of the projectile 2s state vs time in au in a 4 keV He^{2+} -Hydrogen atom collision at $b=0.2$ au

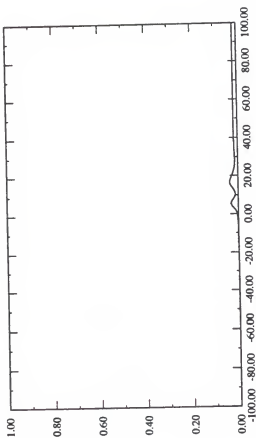


Figure 9-3: Löwdin population of the projectile $2p_x$ state vs time
in au in a 4 keV He^{2+} -Hydrogen atom collision at $b=0.2$ au

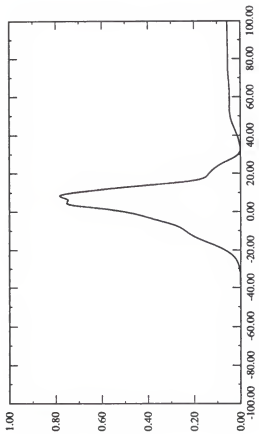


Figure 9-4: Lüwdin population of the projectile $2p_z$ state vs time
in au in a 4 keV He^{2+} -Hydrogen atom collision at $b=0.2$ au

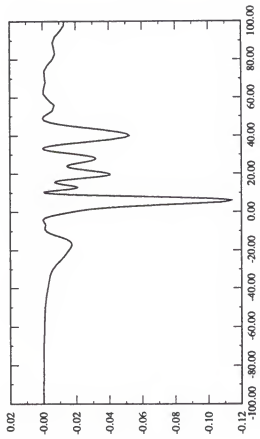


Figure 9-5: Alignment parameter vs time in au in a 4 keV He^{2+} -Hydrogen atom collision at $b=0.2$ au

CHAPTER 10

APPLICATIONS III: THE HYDROGEN ATOM-HYDROGEN ATOM SYSTEM

A third system of interest for us is the collision of two Hydrogen atoms in the ground state. This is the first two-electron system which we have investigated. The total excitation integral cross section and the state-to-state integral cross section will be of interest as well as time-dependent properties. We will consider the projectile energy of 1 keV.

Experimental approaches to this system can again be described in the terms of chapter 8. The combination of a crossed beam geometry and a quenched Lyman- α detector allows for the measurement of the 2s excitation and 2s excitation transfer integral cross sections [63, 61]. The experimental results shown are obtained from linear extrapolation of results obtained at 2 keV and 3 keV projectile energies.

In the case of two active electrons the electron spin becomes important and the density matrices for alpha spin and beta spin must be propagated through time. So equations 4.6 and 4.8 become

$$\begin{aligned} i\dot{\mathbf{P}}_0^\alpha(t) &= \mathbf{W}^\alpha(t_0)\mathbf{P}_0^\alpha(t) - \mathbf{P}_0^\alpha(t)\mathbf{W}^\alpha(t_0)^\dagger \\ i\dot{\mathbf{P}}_0^\beta(t) &= \mathbf{W}^\beta(t_0)\mathbf{P}_0^\beta(t) - \mathbf{P}_0^\beta(t)\mathbf{W}^\beta(t_0)^\dagger \end{aligned} \quad (10.1)$$

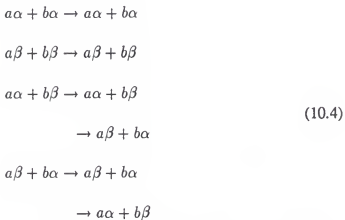
and

$$\begin{aligned} i\dot{\mathbf{Q}}^\alpha(t) &= \mathbf{W}^\alpha(t_0)\mathbf{Q}^\alpha(t) - \mathbf{Q}^\alpha(t)\mathbf{W}^\alpha(t_0)^\dagger + \mathbf{D}^\alpha(t) \\ i\dot{\mathbf{Q}}^\beta(t) &= \mathbf{W}^\beta(t_0)\mathbf{Q}^\beta(t) - \mathbf{Q}^\beta(t)\mathbf{W}^\beta(t_0)^\dagger + \mathbf{D}^\beta(t) \end{aligned} \quad (10.2)$$

where

$$\begin{aligned} W^\alpha &= S^{-1} F^\alpha [P_0^\alpha, P_0^\beta] \\ W^\beta &= S^{-1} F^\beta [P_0^\alpha, P_0^\beta] \end{aligned} \quad (10.3)$$

A number of possible reactions must be considered in the calculation of the excitation cross sections in the Hydrogen atom-Hydrogen atom system. These possibilities reflect the lack of selection of the initial spin state and of analysis of the final spin state in experimental results, and the fact that the projectile and target nuclei are identical. The electronic spin states could proceed from an initial state in which the projectile has an electron in either the alpha spin state or the beta spin state to a final state in which the projectile has an electron of either the same spin state or opposite spin state as the initial state. The possible spin states of the initial states and the final states to the right of the arrow may be summarized by the transitions



where a represents the projectile nucleus and b represents the target nucleus. Therefore, to obtain the appropriate excitation cross section for target hydrogen atom we must average cross sections over initial spin states and add over final

spin states. In particular, for electronic excitation we must add the cross section $\sigma(a\alpha + b\beta \rightarrow a\alpha + b\beta)$, for excitation to the final state with the same electron spins as the initial spin state, to the cross section $\sigma(a\alpha + b\beta \rightarrow a\beta + b\alpha)$, for excitation to the final state with opposite electron spins at the nuclei.

Table 10-1 shows a comparison of experimental and theoretical results for excitation cross sections to 2s and 2p states of the target Hydrogen atom in the collision of a 1 keV projectile Hydrogen atom and a target Hydrogen atom each in their ground electronic state. We use a basis including 1s, 2s, 2p_x, and 2p_z. Hydrogenic orbitals are written as linear combinations of 6 Gaussian orbitals for each center. The electron translation factors are not included in the calculation of electron integrals. However, due to the cancellation of the so-called spurious coupling by the ETF's in the formalism, the electronic populations do go to constant values at the final time. The straight line trajectory is used insofar as previous work shows that the calculation of integral cross sections would not be affected by the use of a zero potential instead of the averaged effective potential at this energy.

We see in Table 10-1 that our 2s state-to-state excitation integral cross section result agrees well with the experiments and the theoretical results of Shingal *et al.* [12]. The disagreement with the result of McLaughlin and Bell [11] is quite sizable and raises questions regarding their procedure. In general, it is fair to say that the agreement of our result with those of other theories is reasonable. At

Table 10.1: A comparison of experiment and theory for excitation integral cross section at 1 keV.

State	H(1s) + H(1s) Integral Excitation Cross Section (10^{-18} cm^2) (ZP)				Experiment
	Theory				
	Present Work	M & B [11]	S <i>et al.</i> [12]	H <i>et al.</i> [61]	M <i>et al.</i> [63]
2s	5.61	0.25	6.5	$3.6 \pm 20\%$	$9.0 \pm 20\%$
2p	4.30	0.56	17	NA	NA

the same time, the agreement with experiment seems quite good for the limited experimental data that are available.

We now move on to consider time-dependent properties in the Hydrogen atom-Hydrogen atom collision. Again we use the same collision conditions for the examination of time-dependent properties as in the preceding two chapters. In this case, we have a 1 keV projectile Hydrogen atom colliding with a target Hydrogen at a an impact parameter of 0.2 au. Figure 10-1 through Figure 10-8 show the time evolution of the electronic populations in spin state alpha in this collision system. Populations settle into constant values for large times. Here the target atom is taken to initially have an electron of alpha spin and the projectile is taken to have an electron in spin state beta. During the interaction the electron spins may get exchanged, and the projectile has a finite probability for flipping its spin state form beta to alpha. We notice the characteristic oscillatory behavior of the electronic populations as a function of time. In this case the excitation is predominantly to the $2p_x$ state. The beta spin electronic populations have very similar structure.

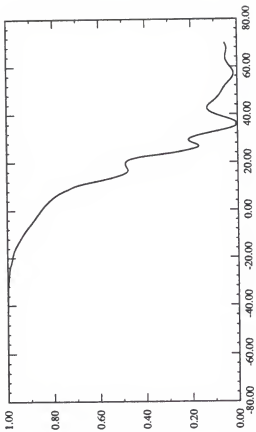


Figure 10-1: Löwdin population for alpha spin of the target 1s state vs time in au for a 1 keV Hydrogen atom-Hydrogen atom collision, at $b=0.2$ au

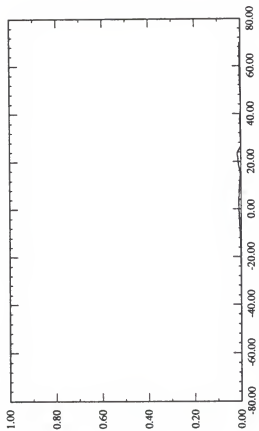


Figure 10-2: Löwdin population for alpha spin of the target 2s state vs time in au for a 1 keV Hydrogen atom-Hydrogen atom collision, at $b=0.2$ au

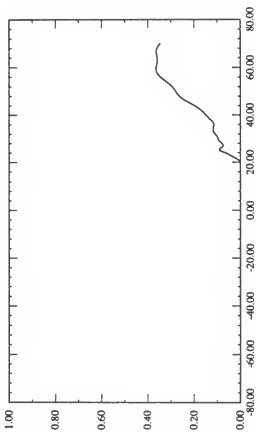


Figure 10-3: Lowdin population for alpha spin of the target $2p_x$ static vs time in au for a 1 keV Hydrogen atom-Hydrogen atom collision, at $b=0.2$ au

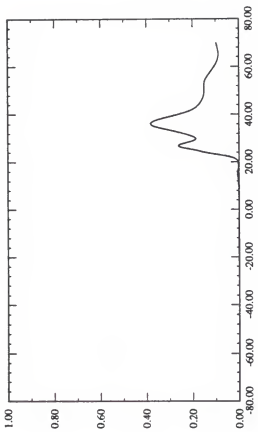


Figure 10-4: Löwdin population for alpha spin of the target $2p_z$ state vs time in au for a 1 keV Hydrogen atom-Hydrogen atom collision, at $b=0.2$ au

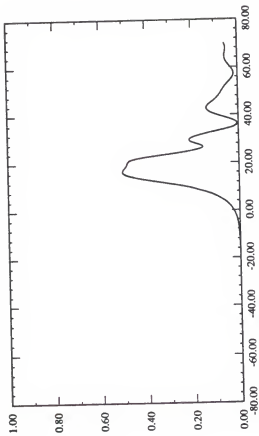


Figure 10-5: Löwdin population for alpha spin of the projectile 1s state vs time in au for a 1 keV Hydrogen atom-Hydrogen atom collision, at $b=0.2$ au

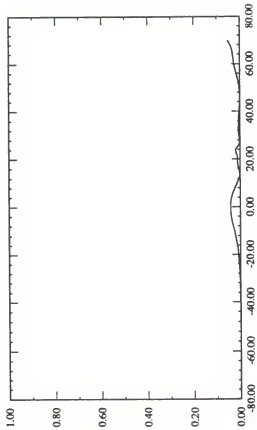


Figure 10-6: Löwdin population for alpha spin of the projectile 2s state vs time in au for a 1 keV Hydrogen atom-Hydrogen atom collision, at $b=0.2$ au

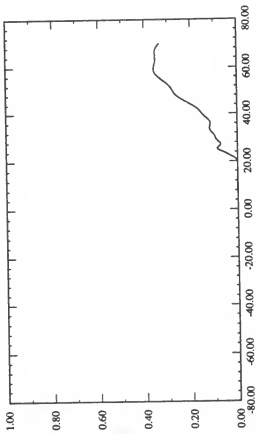


Figure 10-7: Löwdin population for alpha spin of the projectile $2p_x$ state vs time in au for a 1 keV Hydrogen atom-Hydrogen atom collision, at $b=0.2$ au

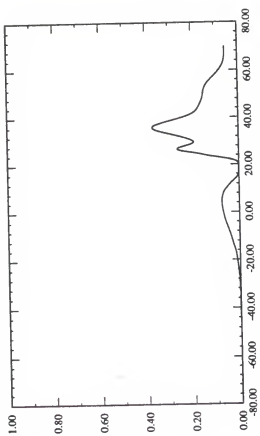


Figure 10-8: Löwdin population for alpha spin of the projectile $2p_z$ state vs time in au for a 1 keV Hydrogen atom-Hydrogen atom collision, at $b=0.2$ au

CHAPTER 11 CONCLUSIONS AND DISCUSSION

The goal of this study has been to develop a methodology to explore in detail the dynamics of electron transfer in ion-atom and atom-atom collisions. Time-dependent quantities describing these phenomena have been of particular interest for gaining detailed insight. A formalism has been developed within time-dependent Hartree-Fock theory for the propagation of electronic density matrices through time while coupling the electronic and atomic core degrees of freedom. The eikonal representation has been used to develop the form of the interaction potential between colliding atoms. An averaged effective potential has been introduced to ensure time reversal invariance of the potential. A temporal linearization procedure was shown to provide a method for solution of the electronic density matrix equations and to ensure the accuracy of this solution. Time-dependent electronic populations and polarization parameters have been introduced and calculated to allow for the detailed description of the collisional process. Electron translation factors have been included in the calculation of electron integrals to properly describe fast collisions, and the effect of the choice of basis set has been assessed.

A new computer code in Fortran77 has been written to efficiently calculate all the necessary components appearing in the integration of the equations of the time-

dependent density matrix formalism. The flow diagram for the time-dependent density matrix computer code is presented in Appendix C. The time-dependent density matrix program package has provided calculations on three systems to determine the validity of the technique as well as to investigate the behavior of the time-dependent properties we have developed. Calculation of charge transfer integral cross sections, state-to-state integral cross sections, differential cross sections, and integral alignments in the proton-Hydrogen atom system over three orders of magnitude in projectile energy have shown a high degree of agreement between the present theoretical results and those of experiment and other theories. The calculation of time-dependent electronic populations and polarization parameters for this system have provided a unique insight into its detailed mechanism of electron transfer.

Calculation of charge transfer integral cross section and state-to-state integral cross section in the Helium(2+)-Hydrogen atom system have shown good agreement with experiment and other theories for projectile energies at which comparisons are available. Again, the calculation of time-dependent electronic populations and polarization parameters have provided unique insights.

The Hydrogen atom-Hydrogen atom system, with two active electron, has also been investigated. The calculation of state-to-state integral excitation cross sections has shown good agreement with available experimental data. The incorporation of two-electron integrals in the time propagation extends the scope of

the application of the time-dependent density matrix code to many active electrons. Time-dependent properties in this system again have provided unique insight into the collisional electron transfer process.

The formalism of time-dependent density matrix calculations is seen to admit to a straightforward interpretation of collision phenomena. The separation of fast and slow degrees of freedom allows for a convenient scheme for optimizing the efficiency of the time propagation algorithm. The ability to propagate the density matrix through time with varying time steps allows the computation to concentrate more time steps in the region of the collision in which most of the change in the electron density is occurring. The definition of a reference density allows for the determination of the amount of change occurring over any given time step by separately treating the oscillations in electronic densities due to relaxation of the system for fixed nuclear positions. The explicit elimination of gradient coupling due to the motion of the cores by means of electron translation factors, assures that the electronic population for each state goes asymptotically to a constant value. This property of our approach permits a detailed assessment of the role of electron translation factors as a function of projectile energy.

Conclusions can be reached based on the research presented here, pertaining to the role of the electron translation factor in the calculation of state-to-state integral cross sections and integral alignments. Our research indicates that ETFs may be neglected in the calculation of state-to-state integral cross sections provided the

core velocities are below 0.02 au and provided the spurious asymptotic couplings are cancelled analytically. Further, our research shows that the effect of the inclusion of ETF's is most strongly noticed in the integral alignment at higher core velocities. We are able to conclude that the differential cross section provides the most demanding test of the accuracy of the choice of core trajectory. It has also been found necessary to use the more accurate averaged effective potential for collisions with appreciable integral cross sections at lower projectile energies.

The time-dependent analyses of collisional systems in terms of electronic populations have led to a number of interesting conclusions. It is noted that electronic populations tend to fluctuate during collisions and to settle at a final value only after what can be numerous fluctuations between the colliding nuclei. The final value of the electronic population is a function of the projectile energy and the impact parameter. A change in impact parameter of only 0.2 au can make the difference between complete transfer and no transfer in the proton-Hydrogen atom system for a 10 eV projectile. It is seen that contrary to the concept of orbital locking, introduced for neutral atoms, the alignment of the electronic system also fluctuates during ion-atom collisions. In summary, this study concludes that electronic transitions in ion-atom and atom-atom collisions are not sudden nor are they necessarily one-step processes. Rather, electronic transitions exhibit oscillatory behavior and sometimes quite rapid fluctuations in these collisions.

The time-dependent density matrix can be improved by the inclusion of a variationally determined transition functional calculated in the atomic orbital basis in which the density matrices are written [30]. Enlarged basis sets including d-orbitals can readily be incorporated in the time-dependent density matrix code. The description of nuclear motions can be generalized in practice to include core electrons as well as nuclei. Finally, the method is suitable for the inclusion of more than two cores and could be used for collision phenomena involving diatomics and polyatomics.

APPENDIX A
CALCULATION OF OVERLAP AND HAMILTONIAN
MATRIX ELEMENTS IN THE HYDROGENIC BASIS

In this appendix we write the two-center overlap and one- and two-center Hamiltonian matrix elements for a Hydrogenic basis including 1s, 2s, 2p₁, 2p₀, and 2p₋₁ orbitals on each center. These spherical representations of the p-type functions are related to the Cartesian in the following way

$$\begin{aligned}|2p_x\rangle &= \frac{1}{\sqrt{2}}(|2p_1\rangle + |2p_{-1}\rangle) \\ |2p_y\rangle &= \frac{1}{i\sqrt{2}}(|2p_1\rangle - |2p_{-1}\rangle) \\ |2p_z\rangle &= |2p_0\rangle\end{aligned}\tag{A.1}$$

Integrations are carried out in elliptical coordinates as defined in chapter 7. The centers are referred to as center a and center b and orbitals are referred to by labels with subscripts to denote the center on which the orbital resides. Hence

$$\langle \chi_a | 1s_b \rangle \tag{A.2}$$

represents the overlap between any orbital on center a and the 1s orbital of center b. The expressions for integrals are tabulated as functions of the internuclear separation R and the effective charge of the centers ζ_m . The following integrals are introduced in the interest of compact notation.

$$A(\beta) = \int_{-1}^1 \exp(-\beta\eta) d\eta = \frac{\exp(\beta) - \exp(-\beta)}{\beta} \tag{A.3}$$

$$\begin{aligned} B(\beta) &= \int_{-1}^1 \eta \exp(-\beta\eta) d\eta \\ &= \left(-\frac{1}{\beta} - \frac{1}{\beta^2}\right) \exp(-\beta) + \left(-\frac{1}{\beta} + \frac{1}{\beta^2}\right) \exp(\beta) \end{aligned} \quad (\text{A.4})$$

$$\begin{aligned} C(\beta) &= \int_{-1}^1 \eta^2 \exp(-\beta\eta) d\eta \\ &= \left(-\frac{1}{\beta} - \frac{2}{\beta^2} - \frac{2}{\beta^3}\right) \exp(-\beta) \\ &\quad + \left(\frac{1}{\beta} - \frac{2}{\beta^2} + \frac{2}{\beta^3}\right) \exp(\beta) \end{aligned} \quad (\text{A.5})$$

$$\begin{aligned} D(\beta) &= \int_{-1}^1 \eta^3 \exp(-\beta\eta) d\eta \\ &= \left(-\frac{1}{\beta} - \frac{3}{\beta^2} - \frac{6}{\beta^3} - \frac{6}{\beta^4}\right) \exp(-\beta) \\ &\quad + \left(-\frac{1}{\beta} + \frac{3}{\beta^2} - \frac{6}{\beta^3} + \frac{6}{\beta^4}\right) \exp(\beta) \end{aligned} \quad (\text{A.6})$$

$$\begin{aligned} F(\beta) &= \int_{-1}^1 \eta^4 \exp(-\beta\eta) d\eta \\ &= \left(-\frac{1}{\beta} - \frac{4}{\beta^2} - \frac{12}{\beta^3} - \frac{24}{\beta^4} - \frac{24}{\beta^5}\right) \exp(-\beta) \\ &\quad + \left(\frac{1}{\beta} - \frac{4}{\beta^2} + \frac{12}{\beta^3} - \frac{24}{\beta^4} + \frac{24}{\beta^5}\right) \exp(\beta) \end{aligned} \quad (\text{A.7})$$

$$G(\alpha) = \int_1^\infty \exp(-\alpha\xi) d\xi = \frac{\exp(-\alpha)}{\alpha} \quad (\text{A.8})$$

$$\begin{aligned} H(\alpha) &= \int_1^\infty \xi \exp(-\alpha\xi) d\xi \\ &= \left(\frac{1}{\alpha} + \frac{1}{\alpha^2}\right) \exp(-\alpha) \end{aligned} \quad (\text{A.9})$$

$$J(\alpha) = \int_1^{\infty} \xi^2 \exp(-\alpha\xi) d\xi \quad (\text{A.10})$$

$$= \left(\frac{1}{\alpha} + \frac{2}{\alpha^2} + \frac{2}{\alpha^3} \right) \exp(-\alpha)$$

$$K(\alpha) = \int_1^{\infty} \xi^3 \exp(-\alpha\xi) d\xi \quad (\text{A.11})$$

$$= \left(\frac{1}{\alpha} + \frac{3}{\alpha^2} + \frac{6}{\alpha^3} + \frac{6}{\alpha^4} \right) \exp(-\alpha)$$

$$L(\alpha) = \int_1^{\infty} \xi^4 \exp(-\alpha\xi) d\xi \quad (\text{A.12})$$

$$= \left(\frac{1}{\alpha} + \frac{4}{\alpha^2} + \frac{12}{\alpha^3} + \frac{24}{\alpha^4} + \frac{24}{\alpha^5} \right) \exp(-\alpha)$$

The following is the list of overlap integrals in terms of the above integral. Note that in general

$$\langle \chi_a | \chi_b \rangle = \langle \chi_b | \chi_a \rangle \quad (\text{A.13})$$

as the hydrogenic orbitals are real, so only the first of the pair of forms will be reported. Also if the two orbitals are on the same center they are orthonormal.

$$\langle 1s_a | 1s_b \rangle = \frac{(\sqrt{\zeta_a \zeta_b} R)^3}{4} [A(\beta) J(\alpha) - C(\beta) G(\alpha)] \quad (\text{A.14})$$

$$\alpha = \frac{1}{2}(\zeta_a + \zeta_b)R ; \beta = \frac{1}{2}(\zeta_a - \zeta_b)R$$

$$\langle 1s_a | 2s_b \rangle = \frac{(\sqrt{\zeta_a \zeta_b} R)^3}{8\sqrt{2}} [A(\beta) J(\alpha) - C(\beta) G(\alpha)] \quad (\text{A.15})$$

$$- \frac{\sqrt{\zeta_a^3 \zeta_b^5} R^4}{32\sqrt{2}} [A(\beta) K(\alpha) - B(\beta) J(\alpha) - C(\beta) H(\alpha) + D(\beta) G(\alpha)]$$

$$\alpha = \frac{1}{4}(2\zeta_a + \zeta_b)R ; \beta = \frac{1}{4}(2\zeta_a - \zeta_b)R$$

$$\langle 1s_a | 2p_{0b} \rangle = \frac{\sqrt{\zeta_a^3 \zeta_b^5} R^4}{32\sqrt{2}} [A(\beta)J(\alpha) - C(\beta)G(\alpha) - B(\beta)K(\alpha) + D(\beta)H(\alpha)] \\ \alpha = \frac{1}{4}(2\zeta_a + \zeta_b)R ; \beta = \frac{1}{4}(2\zeta_a - \zeta_b)R \quad (\text{A.16})$$

$$\langle 2s_a | 2s_b \rangle = \frac{\sqrt{\zeta_a^3 \zeta_b^3} R^3}{32} \{ [A(\beta)J(\alpha) - C(\beta)G(\alpha)] - \frac{\zeta_a R}{4} [A(\beta)K(\alpha) \\ + B(\beta)J(\alpha) - C(\beta)H(\alpha) - D(\beta)G(\alpha)] - \frac{\zeta_b R}{4} [A(\beta)K(\alpha) - B(\beta)J(\alpha) \\ - C(\beta)H(\alpha) + D(\beta)G(\alpha)] + \frac{\zeta_a \zeta_b R^2}{16} [A(\beta)L(\alpha) - 2C(\beta)J(\alpha) + F(\beta)G(\alpha)] \} \\ \alpha = \frac{1}{4}(\zeta_a + \zeta_b)R ; \beta = \frac{1}{4}(\zeta_a - \zeta_b)R \quad (\text{A.17})$$

$$\langle 2s_a | 2p_{0b} \rangle = \frac{\sqrt{\zeta_a^3 \zeta_b^5} R^4}{128} \{ [A(\beta)J(\alpha) - C(\beta)G(\alpha) - B(\beta)K(\alpha) \\ + D(\beta)H(\alpha)] - \frac{\zeta_a R}{4} [A(\beta)K(\alpha) + B(\beta)J(\alpha) - C(\beta)H(\alpha) \\ - D(\beta)G(\alpha) - B(\beta)L(\alpha) - C(\beta)K(\alpha) + D(\beta)J(\alpha) \\ + F(\beta)H(\alpha)] \} \quad (\text{A.18})$$

$$\alpha = \frac{1}{4}(\zeta_a + \zeta_b)R ; \beta = \frac{1}{4}(\zeta_a - \zeta_b)R$$

$$\langle 2p_{1a} | 2p_{1b} \rangle = \frac{\sqrt{\zeta_a^5 \zeta_b^5} R^5}{1024} [A(\beta)L(\alpha) - C(\beta)L(\alpha) - A(\beta)J(\alpha) \\ + F(\beta)J(\alpha) + C(\beta)G(\alpha) - F(\beta)G(\alpha)] \quad (\text{A.19}) \\ \alpha = \frac{1}{4}(\zeta_a + \zeta_b)R ; \beta = \frac{1}{4}(\zeta_a - \zeta_b)R$$

$$\langle 2p_{0a} | 2p_{0b} \rangle = \frac{\sqrt{\zeta_a^5 \zeta_b^5} R^5}{512} [A(\beta)J(\alpha) - C(\beta)G(\alpha) - C(\beta)L(\alpha) + F(\beta)J(\alpha)]$$

$$\alpha = \frac{1}{4}(\zeta_a + \zeta_b)R ; \beta = \frac{1}{4}(\zeta_a - \zeta_b)R \quad (\text{A.20})$$

All other overlap integrals are zero from integration over the φ variable. The following list contains the non-zero one-electron Hamiltonian matrix elements.

$$\langle 1s_a | \hat{H} | 1s_b \rangle = E_{1s_b} \langle 1s_a | 1s_b \rangle - \frac{\sqrt{\zeta_a^5 \zeta_b^3} R^2}{2} [A(\beta)H(\alpha) - B(\beta)G(\alpha)] \quad (\text{A.21})$$

$$\alpha = \frac{1}{2}(\zeta_a + \zeta_b)R ; \beta = \frac{1}{2}(\zeta_a - \zeta_b)R$$

$$\begin{aligned} \langle 2s_a | \hat{H} | 1s_b \rangle &= \langle 2s_a | 1s_b \rangle E_{1s_b} - \frac{\sqrt{\zeta_a^5 \zeta_b^3} R^2}{4\sqrt{2}} \{ A(\beta)H(\alpha) \\ &\quad - B(\beta)G(\alpha) - \frac{\zeta_a R}{4} [A(\beta)J(\alpha) - C(\beta)G(\alpha)] \} \end{aligned} \quad (\text{A.22})$$

$$\alpha = \frac{1}{4}(\zeta_a + 2\zeta_b)R ; \beta = \frac{1}{4}(\zeta_a - 2\zeta_b)R$$

$$\begin{aligned} \langle 2p_{0a} | \hat{H} | 1s_b \rangle &= \langle 2p_{0a} | 1s_b \rangle E_{1s_b} - \frac{\sqrt{\zeta_a^7 \zeta_b^3} R^3}{16\sqrt{2}} [A(\beta)H(\alpha) \\ &\quad - B(\beta)G(\alpha) + B(\beta)J(\alpha) - C(\beta)H(\alpha)] \end{aligned} \quad (\text{A.23})$$

$$\alpha = \frac{1}{4}(\zeta_a + 2\zeta_b)R ; \beta = \frac{1}{4}(\zeta_a - \zeta_b)R$$

$$\begin{aligned}
\langle 2s_a | \hat{H} | 2s_b \rangle &= \langle 2s_a | 2s_b \rangle E_{2s_b} - \frac{\sqrt{\zeta_a^5 \zeta_b^3} R^2}{16} \{ A(\beta) H(\alpha) \\
&\quad - B(\beta) G(\alpha) - \frac{\zeta_a R}{4} [A(\beta) J(\alpha) - C(\beta) G(\alpha)] - \frac{\zeta_b R}{4} [A(\beta) J(\alpha) \\
&\quad - 2B(\beta) H(\alpha) + C(\beta) G(\alpha)] + \frac{\zeta_a \zeta_b R^2}{16} [A(\beta) K(\alpha) - B(\beta) J(\alpha) \\
&\quad - C(\beta) H(\alpha) + D(\beta) G(\alpha)] \}
\end{aligned} \tag{A.24}$$

$$\begin{aligned}
\alpha &= \frac{1}{4} (\zeta_a + \zeta_b) R ; \beta = \frac{1}{4} (\zeta_a - \zeta_b) R \\
\langle 2p_{0a} | \hat{H} | 2s_b \rangle &= \langle 2p_{0a} | 2s_b \rangle E_{2s_b} - \frac{\sqrt{\zeta_a^7 \zeta_b^3} R^3}{64} \{ A(\beta) H(\alpha) \\
&\quad - B(\beta) G(\alpha) + B(\beta) J(\alpha) - C(\beta) H(\alpha) - \frac{\zeta_b R}{4} [A(\beta) J(\alpha) \\
&\quad - 2B(\beta) H(\alpha) + C(\beta) G(\alpha) + B(\beta) K(\alpha) - 2C(\beta) J(\alpha) \\
&\quad + D(\beta) H(\alpha)] \}
\end{aligned} \tag{A.25}$$

$$\begin{aligned}
\alpha &= \frac{1}{4} (\zeta_a + \zeta_b) R ; \beta = \frac{1}{4} (\zeta_a - \zeta_b) R \\
\langle 2p_{0a} | \hat{H} | 2p_{0b} \rangle &= \langle 2p_{0a} | 2p_{0b} \rangle E_{2p_{0b}} - \frac{\sqrt{\zeta_a^7 \zeta_b^5} R^4}{256} [A(\beta) H(\alpha) \\
&\quad - B(\beta) G(\alpha) - C(\beta) K(\alpha) + D(\beta) J(\alpha)]
\end{aligned} \tag{A.26}$$

$$\begin{aligned}
\alpha &= \frac{1}{4} (\zeta_a + \zeta_b) R ; \beta = \frac{1}{4} (\zeta_a - \zeta_b) R \\
\langle 2p_{1a} | \hat{H} | 2p_{1b} \rangle &= \langle 2p_{1a} | 2p_{1b} \rangle E_{2p_{1b}} - \frac{\sqrt{\zeta_a^7 \zeta_b^5} R^4}{512} [B(\beta) G(\alpha) \\
&\quad - A(\beta) H(\alpha) + A(\beta) K(\alpha) - B(\beta) J(\alpha) + C(\beta) H(\alpha) - D(\beta) G(\alpha) \\
&\quad - C(\beta) K(\alpha) + D(\beta) J(\alpha)]
\end{aligned} \tag{A.27}$$

$$\alpha = \frac{1}{4} (\zeta_a + \zeta_b) R ; \beta = \frac{1}{4} (\zeta_a - \zeta_b) R$$

$$\langle 1s_a | \hat{H} | 1s_a \rangle = E_{1s_a} - \frac{\zeta_a^3 \zeta_b R^2}{2} [A(\beta)H(\alpha) + B(\beta)G(\alpha)] \quad (\text{A.28})$$

$$\alpha = \beta = \zeta_a R$$

$$\begin{aligned} \langle 2s_a | \hat{H} | 1s_b \rangle &= -\frac{\zeta_a^3 \zeta_b R^2}{4\sqrt{2}} \{ A(\beta)H(\alpha) + B(\beta)G(\alpha) \\ &\quad - \frac{\zeta_a R}{2} [A(\beta)J(\alpha) + 2B(\beta)H(\alpha) + C(\beta)G(\alpha)] \} \\ \alpha = \beta &= \frac{3}{4} \zeta_a R \end{aligned} \quad (\text{A.29})$$

$$\begin{aligned} \langle 2p_{0a} | \hat{H} | 1s_a \rangle &= -\frac{\zeta_a^4 \zeta_b R^3}{16\sqrt{2}} \{ A(\beta)H(\alpha) + B(\beta)G(\alpha) \\ &\quad B(\beta)J(\alpha) + C(\beta)H(\alpha) \} \\ \alpha = \beta &= \frac{3}{4} \zeta_a R \end{aligned} \quad (\text{A.30})$$

$$\begin{aligned} \langle 2s_a | \hat{H} | 2s_a \rangle &= E_{2s_a} - \frac{\zeta_a^3 \zeta_b R^2}{16} \{ A(\beta)H(\alpha) + B(\beta)G(\alpha) \\ &\quad - \frac{\zeta_a R}{2} [A(\beta)J(\alpha) + 2B(\beta)H(\alpha) + C(\beta)G(\alpha)] \\ &\quad + \frac{\zeta_a^2 R^2}{16} [A(\beta)K(\alpha) + 3B(\beta)J(\alpha) + 3C(\beta)H(\alpha) + D(\beta)G(\alpha)] \} \\ \alpha = \beta &= \frac{1}{2} \zeta_a R \end{aligned} \quad (\text{A.31})$$

$$\begin{aligned} \langle 2s_a | \hat{H} | 2p_{0a} \rangle &= -\frac{\zeta_a^4 \zeta_b R^3}{64} \{ A(\beta)H(\alpha) + B(\beta)G(\alpha) \\ &\quad + B(\beta)J(\alpha) + C(\beta)H(\alpha) - \frac{\zeta_a R}{4} [A(\beta)J(\alpha) + 2B(\beta)H(\alpha) \\ &\quad + C(\beta)G(\alpha) + B(\beta)K(\alpha) + 2C(\beta)J(\alpha) + D(\beta)H(\alpha)] \} \end{aligned} \quad (\text{A.32})$$

$$\alpha = \beta = \frac{1}{2} \zeta_a R$$

$$\langle 2p_{0a} | \hat{H} | 2p_{0a} \rangle = E_{2p_a} - \frac{\zeta_a^5 \zeta_b R^4}{256} [A(\beta)H(\alpha) + B(\beta)G(\alpha) \\ 2B(\beta)J(\alpha) + 2C(\beta)H(\alpha) + C(\beta)K(\alpha) + D(\beta)J(\alpha)] \quad (\text{A.33})$$

$$\alpha = \beta = \frac{1}{2}\zeta_a R$$

$$\langle 2p_{1a} | \hat{H} | 2p_{1a} \rangle = E_{2p_a} - \frac{\zeta_a^5 \zeta_b R^4}{512} [-A(\beta)H(\alpha) - B(\beta)G(\alpha) \\ + A(\beta)K(\alpha) + B(\beta)J(\alpha) + C(\beta)H(\alpha) + D(\beta)G(\alpha) \\ - C(\beta)K(\alpha) - D(\beta)J(\alpha)] \quad (\text{A.34})$$

$$\alpha = \beta = \frac{1}{2}\zeta_a R$$

APPENDIX B
CALCULATION OF ONE-ELECTRON INTEGRALS OVER
GAUSSIANS INCLUDING ELECTRON TRANSLATION FACTORS

In this appendix we present the two-center overlap matrix elements and the two-center one-electron Hamiltonian matrix elements in a basis of Gaussian orbitals including electron translation factors. The general problem under consideration is the evaluation of an integral of the form

$$I = \int d^3r f^*(\vec{r}) \exp(i\vec{q} \cdot \vec{r}) g(\vec{r} + \vec{R}) \quad (\text{B.1})$$

We consider the case in which f and g are real Gaussian functions and $\exp(i\vec{q} \cdot \vec{r})$ corresponds to an ETF. The integration is carried out in Cartesian coordinates and Gaussians of differing angular momenta are related to each other by differentiation with respect to the coordinates of their centers. We consider s-, p-, and d-type Gaussians which are defined by the following relations

$$\begin{aligned} g_s(\alpha, \vec{r}_{mj}) &= \left(\frac{2\alpha}{\pi}\right)^{\frac{3}{4}} \exp(-\alpha r_{mj}^2) \\ g_{p_\zeta}(\alpha, \vec{r}_{mj}) &= \frac{1}{\sqrt{\alpha}} \left[\frac{d}{d\zeta_m} g_s(\alpha, \vec{r}_{mj}) \right] \\ g_{d_{\zeta\eta}}(\alpha, \vec{r}_{mj}) &= \frac{1}{\sqrt{\alpha}} \left[\frac{d}{d\eta_m} g_{p_\zeta}(\alpha, \vec{r}_{mj}) \right] \end{aligned} \quad (\text{B.2})$$

As discussed in chapter 7, we need the two-center overlap integrals which are

$$\begin{aligned}
 I_{s,s} &= \int d^3 r_j g_s(\alpha, \vec{r}_{mj}) \exp(i\vec{q} \cdot \vec{r}_j) g_s(\beta, \vec{r}_{nj}) \\
 &= (\frac{2}{\kappa})^{\frac{3}{2}} (\alpha\beta)^{\frac{3}{4}} K \exp(-\frac{q^2}{4\kappa} + i\vec{q} \cdot \vec{R}_p) \\
 &\quad \kappa = \alpha + \beta ; \quad \vec{R}_p = \frac{\alpha \vec{R}_m + \beta \vec{R}_n}{\kappa} ; \\
 &\quad K = \exp[(\frac{-\alpha\beta}{\kappa})(\vec{R}_m - \vec{R}_n)^2]
 \end{aligned} \tag{B.3}$$

$$\begin{aligned}
 I_{p_\zeta, s} &= \int d^3 r_j g_{p_\zeta}(\alpha, \vec{r}_{mj}) \exp(i\vec{q} \cdot \vec{r}_j) g_s(\beta, \vec{r}_{nj}) \\
 &= \frac{1}{\sqrt{\alpha}} [-(\frac{2\alpha\beta}{\kappa})(\zeta_m - \zeta_n) + \frac{i q_\zeta \alpha}{\kappa}] I_{s,s}
 \end{aligned} \tag{B.4}$$

$$\begin{aligned}
 I_{s, p_\zeta} &= \int d^3 r_j g_s(\alpha, \vec{r}_{mj}) \exp(i\vec{q} \cdot \vec{r}_j) g_{p_\zeta}(\beta, \vec{r}_{nj}) \\
 &= \frac{1}{\sqrt{\beta}} [(\frac{2\alpha\beta}{\kappa})(\zeta_m - \zeta_n) + \frac{i q_\zeta \beta}{\kappa}] I_{s,s}
 \end{aligned} \tag{B.5}$$

$$\begin{aligned}
 I_{p_\zeta, p_\eta} &= \int d^3 r_j g_{p_\zeta}(\alpha, \vec{r}_{mj}) \exp(i\vec{q} \cdot \vec{r}_j) g_{p_\eta}(\beta, \vec{r}_{nj}) \\
 &= \frac{1}{\sqrt{\alpha\beta}} \{ \frac{2\alpha\beta}{\kappa} \delta_{\zeta\eta} \\
 &\quad + [-\frac{2\alpha\beta}{\kappa} (\zeta_m - \zeta_n) + \frac{i q_\zeta \alpha}{\kappa}] [\frac{2\alpha\beta}{\kappa} (\eta_m - \eta_n) + \frac{i q_\eta \beta}{\kappa}] \} I_{s,s}
 \end{aligned} \tag{B.6}$$

$$\begin{aligned}
 I_{d_{\zeta\eta}, s} &= \int d^3 r_j g_{d_{\zeta\eta}}(\alpha, \vec{r}_{mj}) \exp(i\vec{q} \cdot \vec{r}_j) g_s(\beta, \vec{r}_{nj}) \\
 &= \frac{1}{\alpha} \{ (\frac{-2\alpha\beta}{\kappa}) \delta_{\zeta\eta} \\
 &\quad + [-(\frac{2\alpha\beta}{\kappa})(\zeta_m - \zeta_n) + \frac{i q_\zeta \alpha}{\kappa}] [-(\frac{2\alpha\beta}{\kappa})(\eta_m - \eta_n) + \frac{i q_\eta \alpha}{\kappa}] \} I_{s,s}
 \end{aligned} \tag{B.7}$$

$$\begin{aligned}
 I_{s, d_{\zeta\eta}} &= \int d^3 r_j g_s(\alpha, \vec{r}_{mj}) \exp(i\vec{q} \cdot \vec{r}_j) g_{d_{\zeta\eta}}(\beta, \vec{r}_{nj}) \\
 &= \frac{1}{\beta} \{ (\frac{-2\alpha\beta}{\kappa}) \delta_{\zeta\eta} \\
 &\quad + [(\frac{2\alpha\beta}{\kappa})(\zeta_m - \zeta_n) + \frac{i q_\zeta \beta}{\kappa}] [(\frac{2\alpha\beta}{\kappa})(\eta_m - \eta_n) + \frac{i q_\eta \beta}{\kappa}] \} I_{s,s}
 \end{aligned} \tag{B.8}$$

$$\begin{aligned}
I_{d_{\zeta\rho}, p_\eta} &= \int d^3 r_j g_{d_{\zeta\rho}}(\alpha, \vec{r}_{mj}) \exp(i\vec{q} \cdot \vec{r}_j) g_{p_\eta}(\beta, \vec{r}_{nj}) \\
&= \frac{1}{\alpha\sqrt{\beta}} \left\{ \left[\frac{-4\alpha^2\beta^2}{\kappa^2} (\delta_{\zeta\rho}\Delta_\eta + \Delta_\zeta\delta_{\eta\rho}) \right. \right. \\
&\quad + \frac{2i\alpha\beta}{\kappa^2} (\alpha q_\zeta\delta_{\eta\rho} - \beta q_\eta\delta_{\zeta\rho}) \\
&\quad + \left. \left\{ \left(\frac{2\alpha\beta}{\kappa} \right) \delta_{\zeta\eta} + \left[\frac{-4\alpha^2\beta^2}{\kappa^2} \Delta_\zeta\Delta_\eta - \frac{\alpha\beta q_\zeta q_\eta}{\kappa^2} + \frac{2i\alpha\beta}{\kappa^2} (\alpha q_\zeta\Delta_\eta - \beta q_\eta\Delta_\zeta) \right] \right\} \times \right. \\
&\quad \left. \left. \left[\frac{-2\alpha\beta}{\kappa} \Delta_\rho + \frac{i q_\rho \alpha}{\kappa} \right] \right] \right\} I_{s,s} \\
\Delta_\sigma &= \sigma_m - \sigma_n
\end{aligned} \tag{B.9}$$

$$\begin{aligned}
I_{p_\zeta, d_{\eta\rho}} &= \int d^3 r_j g_{p_\zeta}(\alpha, \vec{r}_{mj}) \exp(i\vec{q} \cdot \vec{r}_j) g_{d_{\eta\rho}}(\beta, \vec{r}_{nj}) \\
&= \frac{1}{\beta\sqrt{\alpha}} \left\{ \left[\frac{4\alpha^2\beta^2}{\kappa^2} (\delta_{\zeta\rho}\Delta_\eta + \Delta_\zeta\delta_{\eta\rho}) \right. \right. \\
&\quad + \frac{2i\alpha\beta}{\kappa^2} (-\alpha q_\zeta\delta_{\eta\rho} + \beta q_\eta\delta_{\zeta\rho}) \\
&\quad + \left. \left\{ \left(\frac{2\alpha\beta}{\kappa} \right) \delta_{\zeta\eta} + \left[\frac{-4\alpha^2\beta^2}{\kappa^2} \Delta_\zeta\Delta_\eta - \frac{\alpha\beta q_\zeta q_\eta}{\kappa^2} + \frac{2i\alpha\beta}{\kappa^2} (\alpha q_\zeta\Delta_\eta - \beta q_\eta\Delta_\zeta) \right] \right\} \times \right. \\
&\quad \left. \left. \left[\frac{2\alpha\beta}{\kappa} \Delta_\rho + \frac{i q_\rho \beta}{\kappa} \right] \right] \right\} I_{s,s}
\end{aligned} \tag{B.10}$$

$$\begin{aligned}
I_{d_{\zeta\rho}, d_{\eta\sigma}} &= \int d^3r_j g_{d_{\zeta\rho}}(\alpha, \vec{r}_{mj}) \exp(i\vec{q} \cdot \vec{r}_j) g_{d_{\eta\sigma}}(\beta, \vec{r}_{nj}) \\
&= \frac{1}{\alpha\beta} \left\{ \frac{4\alpha^2\beta^2}{\kappa^2} (\delta_{\zeta\rho}\delta_{\eta\sigma} + \delta_{\zeta\sigma}\delta_{\eta\rho}) \right. \\
&\quad + \left[\frac{4\alpha^2\beta^2}{\kappa^2} (\delta_{\zeta\sigma}\Delta_\eta + \Delta_\zeta\delta_{\eta\sigma}) - \frac{2i\alpha\beta}{\kappa^2} (\alpha q_\zeta\delta_{\eta\sigma} - \beta q_\eta\delta_{\zeta\sigma}) \right] \left[\frac{-2\alpha\beta}{\kappa} \Delta_\rho + \frac{i q_\rho \alpha}{\kappa} \right] \\
&\quad + \left[\frac{2\alpha\beta}{\kappa} \delta_{\zeta\eta} - \frac{4\alpha^2\beta^2}{\kappa^2} \Delta_\zeta\Delta_\eta - \frac{\alpha\beta q_\zeta q_\eta}{\kappa^2} + \frac{2i\alpha\beta}{\kappa^2} (\alpha q_\zeta\Delta_\eta - \beta q_\eta\Delta_\zeta) \right] \left[\frac{2\alpha\beta}{\kappa} \delta_{\rho\sigma} \right] \\
&\quad + \left\{ \frac{-4\alpha^2\beta^2}{\kappa^2} \Delta_\zeta\Delta_\eta + \frac{2i\alpha\beta}{\kappa^2} (\alpha q_\zeta\delta_{\eta\rho} - \beta q_\eta\delta_{\zeta\rho}) \right. \\
&\quad + \left[\frac{2\alpha\beta}{\kappa} \delta_{\zeta\eta} - \frac{4\alpha^2\beta^2}{\kappa^2} \Delta_\zeta\Delta_\eta - \frac{\alpha\beta q_\zeta q_\eta}{\kappa^2} \right. \\
&\quad \left. \left. + \frac{2i\alpha\beta}{\kappa^2} (\alpha q_\zeta\Delta_\eta - \beta q_\eta\Delta_\zeta) \right] \left[\frac{-2\alpha\beta}{\kappa} \Delta_\rho + \frac{i q_\rho \alpha}{\kappa} \right] \right\} \times \\
&\quad \left. \left[\frac{2\alpha\beta}{\kappa} \Delta_\sigma + \frac{i q_\sigma \alpha}{\kappa} \right] \right\} I_{s,s}
\end{aligned} \tag{B.11}$$

As discussed in chapter 7, we also need the two-center one-electron kinetic energy operator matrix elements in the Gaussian basis. These elements are as follows

$$\begin{aligned}
T_{s,s} &= [3\alpha - \frac{3\alpha}{\kappa} - \frac{2\alpha^2\beta^2}{\kappa^2} (\vec{R}_m - \vec{R}_n)^2 + \frac{\alpha^2 q^2}{2\kappa^2} \\
&\quad + \frac{2i\alpha^2\beta}{\kappa^2} \vec{q} \cdot (\vec{R}_m - \vec{R}_n)] I_{s,s}
\end{aligned} \tag{B.12}$$

$$\begin{aligned}
T_{p_\zeta, s} &= [3\alpha - \frac{3\alpha}{\kappa} - \frac{2\alpha^2\beta^2}{\kappa^2} (\vec{R}_m - \vec{R}_n)^2 + \frac{\alpha^2 q^2}{2\kappa^2} \\
&\quad + \frac{2i\alpha^2\beta}{\kappa^2} \vec{q} \cdot (\vec{R}_m - \vec{R}_n)] I_{p_\zeta, s} \\
&\quad + [\frac{-4\alpha^{\frac{3}{2}}\beta^2}{\kappa^2} (\zeta_m - \zeta_n) + \frac{2i\alpha^{\frac{3}{2}}\beta q_\zeta}{\kappa^2}] I_{s,s}
\end{aligned} \tag{B.13}$$

$$\begin{aligned}
T_{s,p_\zeta} = & [3\alpha - \frac{3\alpha^2}{\kappa} - \frac{2\alpha^2\beta^2}{\kappa^2}(\vec{R}_m - \vec{R}_n)^2 + \frac{\alpha^2 q^2}{2\kappa^2} \\
& + \frac{2i\alpha^2\beta}{\kappa^2}\vec{q} \cdot (\vec{R}_m - \vec{R}_n)]I_{s,p_\zeta} \\
& + [\frac{4\alpha^2\beta^{\frac{3}{2}}}{\kappa^2}(\zeta_m - \zeta_n) - \frac{2i\alpha^2\sqrt{\beta}q\zeta}{\kappa^2}]I_{s,s}
\end{aligned} \tag{B.14}$$

$$\begin{aligned}
T_{p_\zeta,p_\eta} = & [3\alpha - \frac{3\alpha^2}{\kappa} - \frac{2\alpha^2\beta^2}{\kappa^2}(\vec{R}_m - \vec{R}_n) + \frac{\alpha^2 q^2}{2\kappa^2} \\
& + \frac{2i\alpha^2\beta}{\kappa^2}\vec{q} \cdot (\vec{R}_m - \vec{R}_n)]I_{p_\zeta,p_\eta} \\
& + [\frac{-4\alpha^{\frac{3}{2}}\beta^2}{\kappa^2}(\zeta_m - \zeta_n) + \frac{2i\alpha^{\frac{3}{2}}\beta q\zeta}{\kappa^2}]I_{s,p_\eta} \\
& + [\frac{4\alpha^2\beta^{\frac{3}{2}}}{\kappa^2}(\eta_m - \eta_n) - \frac{2i\alpha^2\sqrt{\beta}q\eta}{\kappa^2}]I_{p_\zeta,s} \\
& + [\frac{4\alpha^{\frac{3}{2}}\beta^{\frac{3}{2}}}{\kappa^2}\delta_{\zeta\eta}]I_{s,s}
\end{aligned} \tag{B.15}$$

$$\begin{aligned}
T_{d_{\zeta\eta},s} = & [3\alpha - \frac{3\alpha^2}{\kappa} - \frac{2\alpha^2\beta^2}{\kappa^2}(\vec{R}_m - \vec{R}_n)^2 + \frac{\alpha^2 q^2}{2\kappa^2} \\
& + \frac{2i\alpha^2\beta}{\kappa^2}\vec{q} \cdot (\vec{R}_m - \vec{R}_n)]I_{d_{\zeta\eta},s} \\
& + [\frac{-4\alpha^{\frac{3}{2}}\beta^2}{\kappa^2}(\eta_m - \eta_n) + \frac{2i\alpha^{\frac{3}{2}}\beta q\eta}{\kappa^2}]I_{p_\zeta,s} \\
& + [\frac{-4\alpha^{\frac{3}{2}}\beta^2}{\kappa^2}(\zeta_m - \zeta_n) + \frac{2i\alpha^{\frac{3}{2}}\beta q\zeta}{\kappa^2}]I_{p_\eta,s} \\
& + [\frac{-4\alpha\beta^2}{\kappa^2}\delta_{\zeta\eta}]I_{s,s}
\end{aligned} \tag{B.16}$$

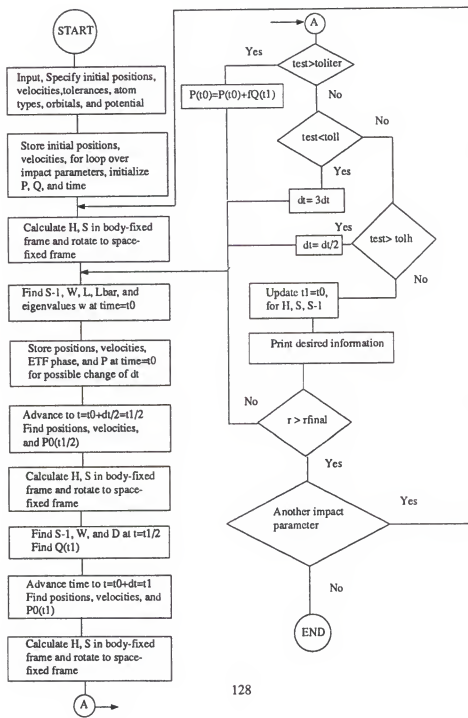
$$\begin{aligned}
T_{s,d_{\zeta\eta}} = & [3\alpha - \frac{3\alpha^2}{\kappa} - \frac{2\alpha^2\beta^2}{\kappa^2}(\vec{R}_m - \vec{R}_n)^2 + \frac{\alpha^2q^2}{2\kappa^2} \\
& + \frac{2i\alpha^2\beta}{\kappa^2}\vec{q}\cdot(\vec{R}_m - \vec{R}_n)]I_{s,d_{\zeta\eta}} \\
& + [\frac{4\alpha^2\beta^{\frac{3}{2}}}{\kappa^2}(\eta_m - \eta_n) - \frac{2i\alpha^2\sqrt{\beta}q_\eta}{\kappa^2}]I_{s,p_\zeta} \\
& + [\frac{4\alpha^2\beta^{\frac{3}{2}}}{\kappa^2}(\zeta_m - \zeta_n) - \frac{2i\alpha^2\sqrt{\beta}q_\zeta}{\kappa^2}]I_{s,p_\eta} \\
& + [\frac{-4\alpha^2\beta}{\kappa^2}\delta_{\zeta\eta}]I_{s,s}
\end{aligned} \tag{B.17}$$

$$\begin{aligned}
T_{d_{\zeta\rho},p_\eta} = & [3\alpha - \frac{3\alpha^2}{\kappa} - \frac{2\alpha^2\beta^2}{\kappa^2}(\vec{R}_m - \vec{R}_n)^2 + \frac{\alpha^2q^2}{2\kappa^2} \\
& + \frac{2i\alpha^2\beta}{\kappa^2}\vec{q}\cdot(\vec{R}_m - \vec{R}_n)]I_{d_{\zeta\rho},p_\eta} \\
& + [\frac{-4\alpha^{\frac{3}{2}}\beta^2}{\kappa^2}(\rho_m - \rho_n) + \frac{2i\alpha^{\frac{3}{2}}\beta q_\rho}{\kappa^2}]I_{p_\zeta,p_\eta} \\
& + [\frac{-4\alpha^{\frac{3}{2}}\beta^2}{\kappa^2}(\zeta_m - \zeta_n) + \frac{2i\alpha^{\frac{3}{2}}\beta q_\zeta}{\kappa^2}]I_{p_\rho,p_\eta} \\
& + [\frac{4\alpha^2\beta^{\frac{3}{2}}}{\kappa^2}(\eta_m - \eta_n) - \frac{2i\alpha^2\sqrt{\beta}q_\eta}{\kappa^2}]I_{d_{\zeta\rho},s} \\
& + [\frac{-4\alpha\beta^2}{\kappa^2}\delta_{\zeta\rho}]I_{s,p_\eta} \\
& + [\frac{4\alpha^{\frac{3}{2}}\beta^{\frac{3}{2}}}{\kappa^2}\delta_{\zeta\eta}]I_{p_\rho,s} \\
& + [\frac{4\alpha^{\frac{3}{2}}\beta^{\frac{3}{2}}}{\kappa^2}\delta_{\eta\rho}]I_{p_\zeta,s}
\end{aligned} \tag{B.18}$$

$$\begin{aligned}
T_{p_\zeta, d_{\eta\rho}} = & [3\alpha - \frac{3\alpha^2}{\kappa} - \frac{2\alpha^2\beta^2}{\kappa^2}(\vec{R}_m - \vec{R}_n)^2 + \frac{\alpha^2 q^2}{2\kappa^2} \\
& - \frac{2i\alpha^2\beta}{\kappa^2}\vec{q} \cdot (\vec{R}_m - \vec{R}_n)]I_{p_\zeta, d_{\eta\rho}} \\
& + [\frac{4\alpha^2\beta^{\frac{3}{2}}}{\kappa^2}(\rho_m - \rho_n) - \frac{2i\alpha^2\sqrt{\beta}q_\rho}{\kappa^2}]I_{p_\zeta, p_\eta} \\
& + [\frac{-4\alpha^{\frac{3}{2}}\beta^2}{\kappa^2}(\zeta_m - \zeta_n) + \frac{2i\alpha^{\frac{3}{2}}\beta q_\zeta}{\kappa^2}]I_{s, d_{\eta\rho}} \\
& + [\frac{4\alpha^2\beta^{\frac{3}{2}}}{\kappa^2}(\eta_m - \eta_n) - \frac{2i\alpha^2\sqrt{\beta}q_\eta}{\kappa^2}]I_{p_\zeta, p_\rho} \\
& + [\frac{4\alpha^{\frac{3}{2}}\beta^{\frac{3}{2}}}{\kappa^2}\delta_{\zeta\rho}]I_{s, p_\eta} \\
& + [\frac{4\alpha^{\frac{3}{2}}\beta^{\frac{3}{2}}}{\kappa^2}\delta_{\zeta\eta}]I_{s, p_\rho} \\
& + [\frac{-4\alpha^2\beta}{\kappa^2}\delta_{\eta\rho}]I_{p_\zeta, s}
\end{aligned} \tag{B.19}$$

$$\begin{aligned}
T_{d_{\zeta\rho}, d_{\eta\sigma}} = & [3\alpha - \frac{3\alpha^2}{\kappa} - \frac{2\alpha^2\beta^2}{\kappa^2}(\vec{R}_m - \vec{R}_n)^2 + \frac{\alpha^2 q^2}{2\kappa^2} \\
& + \frac{2i\alpha^2\beta}{\kappa^2}\vec{q} \cdot (\vec{R}_m - \vec{R}_n)]I_{d_{\zeta\rho}, d_{\eta\sigma}} \\
& + [\frac{-4\alpha^{\frac{3}{2}}\beta^2}{\kappa^2}(\rho_m - \rho_n) + \frac{2i\alpha^{\frac{3}{2}}\beta q_\rho}{\kappa^2}]I_{p_\zeta, d_{\eta\sigma}} \\
& + [\frac{-4\alpha^{\frac{3}{2}}\beta^2}{\kappa^2}(\zeta_m - \zeta_n) + \frac{2i\alpha^{\frac{3}{2}}\beta q_\zeta}{\kappa^2}]I_{p_\rho, d_{\eta\sigma}} \\
& + [\frac{4\alpha^2\beta^{\frac{3}{2}}}{\kappa^2}(\eta_m - \eta_n) - \frac{2i\alpha^2\sqrt{\beta}q_\eta}{\kappa^2}]I_{d_{\zeta\rho}, p_\sigma} \\
& + [\frac{4\alpha^2\beta^{\frac{3}{2}}}{\kappa^2}(\sigma_m - \sigma_n) - \frac{2i\alpha^2\sqrt{\beta}q_\sigma}{\kappa^2}]I_{d_{\zeta\rho}, p_\eta} \\
& + [\frac{-4\alpha\beta^2}{\kappa^2}\delta_{\zeta\rho}]I_{s, d_{\eta\sigma}} \\
& + [\frac{4\alpha^{\frac{3}{2}}\beta^{\frac{3}{2}}}{\kappa^2}\delta_{p_\sigma}]I_{p_\zeta, p_\eta} \\
& + [\frac{4\alpha^{\frac{3}{2}}\beta^{\frac{3}{2}}}{\kappa^2}\delta_{\zeta\eta}]I_{p_\rho, p_\sigma} \\
& + [\frac{4\alpha^{\frac{3}{2}}\beta^{\frac{3}{2}}}{\kappa^2}\delta_{\eta\rho}]I_{p_\zeta, p_\eta} \\
& + [\frac{4\alpha^{\frac{3}{2}}\beta^{\frac{3}{2}}}{\kappa^2}\delta_{\zeta\sigma}]I_{p_\rho, p_\eta} \\
& + [\frac{-4\alpha^2\beta}{\kappa^2}\delta_{\eta\sigma}]I_{d_{\zeta\rho}, s}
\end{aligned} \tag{B.20}$$

APPENDIX C
FLOW CHART OF THE TIME-DEPENDENT
DENSITY MATRIX COMPUTER PROGRAM



REFERENCES

1. A. Dalgarno and H. N. Yadav, Proc. Phys. Soc. **66**, 173 (1952).
2. N. F. Mott and H. S. W. Massey, *The Theory of Atomic Collisions*, Clarendon Press, Oxford, third edition, 1965, chap. 15.
3. G. Hunter and M. Kuriyan, Proc. R. Soc. London **A353**, 575 (1977).
4. G. Hunter and M. Kuriyan, Proc. R. Soc. London **A358**, 321 (1977).
5. N. Grun, A. Muhlhaus, and W. Scheid, J. Phys. B **15**, 4043 (1982).
6. W. Fritsch and C. D. Lin, Phys. Rep. **202**, 1 (1991).
7. M. Kimura and N. F. Lane, Adv. At. Mol. Opt. Phys. **26**, 79 (1990).
8. R. McCarroll, Proc. R. Soc. London **A264**, 547 (1961).
9. D. Rapp and D. Dinwiddie, J. Chem. Phys. **57**, 4919 (1972).
10. D. Rapp, J. Chem. Phys. **58**, 2043 (1973).
11. B. M. McLaughlin and K. L. Bell, J. Phys. B **16**, 3797 (1983).
12. R. Shingal, B. H. Bransden, and D. R. Flower, J. Phys. B **22**, 855 (1989).
13. W. Fritsch, J. Physique **50**, C1 (1989).
14. W. Fritsch and C. D. Lin, Phys. Rev. A **26**, 762 (1982).
15. W. Fritsch and C. D. Lin, Phys. Rev. A **27**, 3361 (1983).
16. W. Fritsch, Phys. Rev. A **38**, 2664 (1988).

17. T. G. Winter and N. F. Lane, Phys. Rev. A **17**, 66 (1978).
18. T. G. Winter and G. J. Hatton, Phys. Rev. A **21**, 793 (1980).
19. M. Kimura and W. R. Thorson, Phys. Rev. A **24**, 1780 (1981).
20. M. Kimura and W. R. Thorson, Phys. Rev. A **24**, 3019 (1981).
21. I. M. Cheshire, D. F. Gallaher, and A. J. Taylor, J. Phys. B **3**, 813 (1970).
22. H. J. Ludde and R. M. Dreizler, J. Phys. B **15**, 2703 (1982).
23. H. J. Ludde and R. M. Dreizler, J. Phys. B **15**, 2713 (1982).
24. R. McCarroll and R. D. Piacentini, J. Phys. B **7**, 1336 (1970).
25. C. Gaussorgues, C. LeSech, F. Masnou-Seeuws, R. McCarrol, and A. Riera, J. Phys. B **8**, 253 (1975).
26. D. A. Micha, J. Chem. Phys. **78**, 7138 (1983).
27. C. D. Stodden and D. A. Micha, Intern. J. Quantum Chem. Symposium **21**, 239 (1987).
28. P. K. Swaminathan, C. D. Stodden, and D. A. Micha, J. Chem. Phys. **90**, 5501 (1989).
29. J. M. Cohen and D. A. Micha, J. Chem. Phys. **97**, 1038 (1992).
30. D. A. Micha and B. Gazdy, Phys. Rev. A **36**, 539 (1987).
31. B. Gazdy and D. A. Micha, Phys. Rev. A **36**, 546 (1987).
32. K. Runge and D. A. Micha, Abstract, Sanibel Symposium, April 1-8, 1989, St. Augustine. "Time-dependent SCF theory of Molecular Interactions".

33. K. Runge and D. A. Micha, Abstract, Sanibel Symposium, March 17-24, 1990, St. Augustine. "Coupling of Electronic and Nuclear Motions in Atomic Collisions using a Time-Dependent MO approach".
34. K. Runge, D. A. Micha, and E. Q. Feng, Intern. J. Quantum Chem. Symposium **24**, 781 (1990).
35. K. Runge and D. A. Micha, Abstract, Sanibel Symposium, March 9-16, 1991, St. Augustine. "Polarization Effects in Ion-Atom Collision Using A Time-Dependent Molecular Orbital Approach".
36. K. Runge and D. A. Micha, Abstract, Sanibel Symposium, March 14-21, 1992, St. Augustine. "Time-Evolution of Electronic Populations and Polarization Parameters in Slow Ion-Atom Collisions".
37. P. Kramer and M. Saraceno, *Geometry of the Time-Dependent Variational Principle in Quantum Mechanics*, Springer, New York, 1981.
38. D. J. Thouless, Nucl. Phys. **21**, 225 (1960).
39. E. Deumens, A. Diz., H. Taylor, and Y. Ohrn, J. Chem. Phys. **96**, 6820 (1992).
40. D. R. Bates and R. McCarroll, Proc. R. Soc. London **A245**, 175 (1958).
41. J. B. Delos, Rev. Mod. Phys. **53**, 287 (1981).
42. G. H. Golub and C. F. V. Loan, *Matrix Computations*, The Johns Hopkins University Press, Baltimore, Maryland, 1989.
43. J. P. Hansen, A. Dubois, and S. E. Nielsen, Phys. Rev. A **44**, 6130 (1991).
44. C. D. Lin, R. Shingal, A. Jain, and W. Fritsch, Phys. Rev. A **39**, 4455 (1989).
45. W. Fritsch and C. D. Lin, Phys. Rep. **202**, 1 (1991).
46. R. Hippler, H. Madeheim, W. Harbich, H. Kleinpoppen, and H. O. Lutz, Phys. Rev. A **38**, 1662 (1988).

47. R. N. Zare, *Angular Momentum*, J. Wiley, New York, 1988.
48. A. Szabo and N. S. Ostlund, *Modern Quantum Chemistry*, McGraw-Hill Inc., New York, 1989.
49. H. Goldstein, *Classical Mechanics*, Addison-Wesley, Reading, Massachusetts, 1980.
50. S. F. Boys, Proc. R. Soc. London A200, 542 (1950).
51. W. J. Hehre, Ditchfield, R. F. Stewart, and J. A. Pople, J. Chem. Phys. 52, 2769 (1970).
52. VMOL is a local version of MOLECULE, a vectorized Gaussian integral computer program, authored by J. Almlöf and P. R. Taylor.
53. R. McWeeny, Acta Cryst. 6, 631 (1953).
54. W. L. Fite, A. C. H. Smith, and R. F. Stebbings, Proc. R. Soc. London A268, 527 (1962).
55. W. L. Fite, R. F. Stebbings, D. G. Hummer, and R. T. Brackmann, Phys. Rev. 119, 663 (1960).
56. G. W. McClure, Phys. Rev. 148, 47 (1966).
57. M. W. Gealy and B. V. Zyl, Phys. Rev. A 36, 3091 (1987).
58. T. Kondow, R. J. Girnius, Y. P. Chong, and W. L. Fite, Phys. Rev. A 10, 1167 (1974).
59. W. E. Kauppila, P. J. O. Teubner, W. L. Fite, and R. J. Girnius, Phys. Rev. A 2, 1759 (1970).
60. R. F. Stebbings, R. A. Young, C. L. Oxley, and H. Ehrhard, Phys. Rev. 138, A1312 (1965).

61. J. Hill, J. Geddes, and H. B. Gilbody, *J. Phys. B* **12**, 2875 (1979).
62. T. J. Morgan, J. Geddes, and H. B. Gilbody, *J. Phys. B* **6**, 2118 (1973).
63. T. J. Morgan, J. Stone, and R. Mayo, *Phys. Rev. A* **22**, 1460 (1980).
64. Y. P. Chong and W. L. Fite, *Phys. Rev. A* **16**, 933 (1977).
65. J. C. Houver, J. Fayeton, and M. Barat, *J. Phys. B* **7**, 1358 (1974).
66. J. H. Newman, J. D. Cogan, D. L. Ziegler, D. E. Nitz, R. D. Rundel, K. A. Smith, and R. F. Stebbings, *Phys. Rev. A* **25**, 2976 (1982).
67. W. L. Nutt, R. W. McCullough, K. Brady, M. B. Shah, and H. B. Gilbody, *J. Phys. B* **11**, 1457 (1978).
68. D. Ceric, D. Dijkkamp, E. Vlieg, and F. J. DeHeer, *J. Phys. B* **18**, 4745 (1985).
69. D. Ceric, R. Hoekstra, F. J. de Heer, and R. Morgenstern, Single electron capture in one-electron systems, in *Electronic and Atomic Collisions*, edited by H. B. Gilbody, W. R. Newell, F. H. Read, and A. C. H. Smith, page 655, Elsevier Science Publishers B. V., North Holland, Amsterdam, 1988.
70. J. E. Bayfield and G. A. Khayrallah, *Phys. Rev. A* **12**, 869 (1975).
71. M. B. Shah and H. B. Gilbody, *J. Phys. B* **11**, 121 (1978).

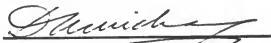
BIOGRAPHICAL SKETCH

Keith Runge was born on Reformation Sunday, October 29, 1961, in Jeanette, Pennsylvania, at about 1:50 am to Rev. Earl Runge and Jacqueline Koch Runge. Earl, then the pastor of Penn Evangelical Lutheran Church in Penn, Pennsylvania, was probably wondering how he would stay awake through the morning and evening services that day. Jackie, oddly enough, was wondering why the clock had so abruptly returned to 1:00 am from 2:00 am less than one hour before. Keith cannot remember what he was wondering. Keith proved to be no more convenient for most of the rest of his life to this date.

At the age of five, Keith moved with his family to Lamartine, Pennsylvania, where his father still resides. He began his elementary education at Salem Elementary School under a promise extorted from his mother. In the midst of sixth grade he was transferred to Keystone Elementary School in Knox, Pennsylvania. He continued in the Keystone School system graduating in May of 1979. He then enrolled in Thiel College in Greenville, Pennsylvania, where his brother Kenneth now resides. Keith graduated from Thiel in May of 1983 with majors in physics, chemistry, and mathematics. During his time at Thiel, he did research projects with Dr. David A. Micha at the University of Florida, Dr. Donald Truhlar at the University of Minnesota, and Dr. Karl Riemann at Argonne National Laboratories. Keith then enrolled in the Lutheran Theological Seminary

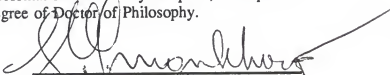
at Gettysburg, Pennsylvania, in the Fall of 1984. After a year at the seminary, he decided to enroll at the University of Florida noting that the prevailing climate was warmer than either Minneapolis or Chicago. Since then, Keith has labored as a graduate student in the Physics Department and this thesis is what he has to show for it.

I certify that I have read this study and that in my opinion it conforms to acceptable standards of scholarly presentation and is fully adequate, in scope and quality, as a dissertation for the degree of Doctor of Philosophy.



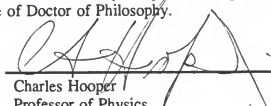
David A. Micha, Chair
Professor of Chemistry and
Physics

I certify that I have read this study and that in my opinion it conforms to acceptable standards of scholarly presentation and is fully adequate, in scope and quality, as a dissertation for the degree of Doctor of Philosophy.



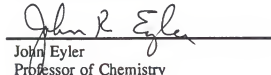
Hendrik J. Monkhorst
Professor of Physics and
Chemistry

I certify that I have read this study and that in my opinion it conforms to acceptable standards of scholarly presentation and is fully adequate, in scope and quality, as a dissertation for the degree of Doctor of Philosophy.



Charles Hooper
Professor of Physics

I certify that I have read this study and that in my opinion it conforms to acceptable standards of scholarly presentation and is fully adequate, in scope and quality, as a dissertation for the degree of Doctor of Philosophy.



John R. Eyler
Professor of Chemistry

I certify that I have read this study and that in my opinion it conforms to acceptable standards of scholarly presentation and is fully adequate, in scope and quality, as a dissertation for the degree of Doctor of Philosophy.



Yngve N. Öhrn
Professor of Chemistry and
Physics

This dissertation was submitted to the Graduate Faculty of the Department of Physics in the College of Liberal Arts and Sciences, and to the Graduate School and was accepted as partial fulfillment of the requirements for the degree of Doctor of Philosophy.

May 1993

Dean, Graduate School